Direct and indirect effects of joint torque inputs during an induced speed analysis of a swinging motion

Sekiya Koike, Tatsuya Ishikawa, Alexander P. Willmott, Neil Bezodis

PII: S0021-9290(19)30069-7
DOI: https://doi.org/10.1016/j.jbiomech.2019.01.032
Reference: BM 9041

To appear in: *Journal of Biomechanics*

Accepted Date: 16 January 2019

Please cite this article as: S. Koike, T. Ishikawa, A.P. Willmott, N. Bezodis, Direct and indirect effects of joint torque inputs during an induced speed analysis of a swinging motion, *Journal of Biomechanics* (2019), doi: https://doi.org/10.1016/j.jbiomech.2019.01.032

Original article

Direct and indirect effects of joint torque inputs during an induced speed analysis of a swinging motion

Sekiya Koike[1], Tatsuya Ishikawa[2], Alexander P. Willmott[3] and Neil Bezodis[4]

[1]Faculty of Health and Sport Sciences, University of Tsukuba, Japan,

[2]Institute of Sport Science, Asics Corporation, Japan

[3]School of Sport and Exercise Science, University of Lincoln, UK

[4]Applied Sports, Technology, Exercise and Medicine Research Centre, Swansea University, UK

Corresponding Author:

Sekiya Koike, Faculty of Health and Sport Sciences, University of Tsukuba,

1-1-1 Tennodai, Tsukuba City, Ibaraki Prefecture, 305-8574, Japan.

Tel: +81 – 29 – 853 – 2677

Fax: +81 – 29 – 853 – 2677

E-mail: koike.sekiya.fp@u.tsukuba.ac.jp

***Keywords*:**

Kinetic chain, Whip-like effect, Dynamic contribution, Cause-and-effect relationship, Rugby kicking

Word Counts: 3997 in manuscript, and 1739 in appendices for supplementary

Abstract

This study proposed a method to quantify direct and indirect effects of the joint torque inputs in the speed-generating mechanism of a swinging motion. Linear and angular accelerations of all segments within a multi-linked system can be expressed as the sum of contributions from a joint torque term, gravitational force term and motion-dependent term (MDT), where the MDT is a nonlinear term consisting of centrifugal force, Coriolis force and a gyroscopic effect moment. Direct effects result from angular accelerations induced by a joint torque at a given instant, whereas indirect effects arise through the MDT induced by joint torques exerted in the past. These two effects were quantified for the kicking-side leg during a rugby place kick. The MDT was the largest contributor to the foot centre of gravity (CG)'s speed at ball contact. Of the factors responsible for generating the MDT, the direct and indirect effects of the hip flexion-extension torque during both the flight phase (from the final kicking foot take-off to support foot contact) and the subsequent support phase (from support foot contact to ball contact) were important contributors to the foot CG's speed at ball contact. The indirect effect of the ankle plantar-dorsal flexion torque and the direct effect of the knee flexion-extension torque during the support phase showed the largest positive and negative contributions to the foot CG's speed at ball contact, respectively. The proposed method allows the identification of which individual joint torque axes are crucial and the timings of joint torque exertion that are used to generate a high speed of the distal point of a multi-linked system.

NOMENCLATURE

$\boldsymbol{V}$	generalised velocity vector consisting of linear and angular velocity vectors for all the segments
$\dot{\boldsymbol{V}}$	generalised acceleration vector
$\boldsymbol{A}_{\boldsymbol{V},\boldsymbol{T}\mathrm{a}}$	coefficient matrix for the joint torque vector
$\boldsymbol{T}_{\mathrm{a}}$	joint torque vector consisting of active torques
$\overline{\boldsymbol{A}}_{\boldsymbol{V},\mathrm{MDT}}(\boldsymbol{V})$	coefficient matrix for the motion-dependent term, which is a function of the generalised velocity vector
$\boldsymbol{A}_{\boldsymbol{V},\boldsymbol{G}}$	coefficient matrix for gravitational force
$\boldsymbol{G}$	gravitational force vector
$\boldsymbol{B}_{\boldsymbol{V},\mathrm{other}}$	vector consisting of the hip-joint acceleration, segment length fluctuation, and constraint joint axial angle fluctuation terms
$\boldsymbol{A}_{\boldsymbol{V},\mathrm{Hip}}$	coefficient matrix for the hip joint acceleration vector
$\ddot{\boldsymbol{x}}_{\mathrm{Hip}}$	hip joint acceleration
$\boldsymbol{A}_{\boldsymbol{V},\boldsymbol{\eta}}$	coefficient matrix for the double derivation of segment length fluctuation vector
$\boldsymbol{\eta}$	vector of segment length fluctuation
$\boldsymbol{A}_{\boldsymbol{V},\boldsymbol{\varphi}}$	coefficient matrix for the double derivation of constraint joint axial angle fluctuation
$\boldsymbol{\varphi}$	vector of constraint joint axial angle fluctuation
$\dot{\boldsymbol{V}}_{\mathrm{Dir}}$	generalised acceleration vector due to the direct effect of joint torque, gravity and other inputs
$\dot{\boldsymbol{V}}_{\mathrm{Indir}}$	generalised acceleration vector due to the indirect effect of joint torque, gravity and other inputs
k	k-th time instant in the discrete-time system
h	any given instant in time between swing start to time k

Δt time interval in the discrete-time system

$\boldsymbol{\Psi_V}$ coefficient matrix for the generalised velocity vector defined as $\boldsymbol{E}_{18} + \Delta t \bar{\boldsymbol{A}}_{\boldsymbol{V},\mathrm{MDT}}(\boldsymbol{V})$

$\boldsymbol{E}_{18}$ unit matrix with eighteen rows and columns

$\widetilde{\boldsymbol{V}}$ measured generalised velocity vector

$\widetilde{\boldsymbol{\Psi}}_{\boldsymbol{V}}$ coefficient matrix for the generalised velocity vector defined as $\boldsymbol{E}_{18} + \Delta t \bar{\boldsymbol{A}}_{\boldsymbol{V},\mathrm{MDT}}(\widetilde{\boldsymbol{V}})$

$\boldsymbol{V}(0)$ initial value of the generalised velocity vector

i subscript expressing segment number (i.e. i=1, thigh; i=2, shank; i=3, foot)

$\boldsymbol{S}_i$ selective matrix extracting the linear velocity vector of segment i from the generalised velocity vector

$\dot{\boldsymbol{x}}_i$ linear velocity vector for the centre of gravity of segment i

$\boldsymbol{e}_i$ unit vector for the linear velocity vector for the centre of gravity of segment i

s_{Dir} speed of segment's centre of gravity induced by direct effect of joint torque inputs

s_{Indir} speed of segment's centre of gravity induced by indirect effect of joint torque inputs

s_i contribution to the speed of segment i's centre of gravity induced by both direct and indirect effects of joint torque inputs

1. Introduction

Quantification of the kinetics underpinning the generation of high distal-point speed in swinging motions has provided knowledge regarding how players exert joint torques to produce distinctive patterns of motion within a multi-linked system. Numerous studies have analysed high-speed swinging motions such as baseball pitching (e.g. Feltner and Dapena, 1986; Feltner, 1989; Fleisig et al., 1995; Fleisig et al., 1996a; Fleisig et al., 1996b), tennis serving (e.g. Elliott et al., 2003; Reid et al., 2007), and soccer kicking (e.g. Lees and Rahnama, 2013; Nunome et al., 2002). Although these studies reveal how players exert joint torques during these motions, it remains unclear exactly how and when the individual joint torques exerted affect the speed of the multi-linked system at ball release or ball contact, because such kinetic analyses have limitations in dealing with the cause-and-effect relationship between joint torque inputs and motion outputs.

Since the human body consists of numerous segments connected via joints which are typically assumed to move with only rotational displacements, human movements are performed through angular displacements at joints to achieve coordinated multiple segment motion. The equation of motion for a multi-linked system (e.g. human body) can be expressed generally in the following form (e.g. Kepple et al., 1997; Koike et al., 2017; Zajac et al., 2002) when ignoring modelling errors:

(Linear and angular accelerations of all segments) or (Angular accelerations of all joints)

= (Joint torque term) + (Gravitational term) + (Motion-dependent term), (1)

where the motion-dependent term (MDT) is a nonlinear term consisting of centrifugal forces, Coriolis forces and gyroscopic effect moments. Equation 1 indicates that segmental motion (i.e. linear and angular accelerations) is induced not only by the joint torque inputs and gravitational force but also by the MDT. Motion can be induced by the

joint forces exerted at individual joints through motion-dependent mechanisms, even when the inputted joint torques are small. These joint forces do not appear directly as a separate term in Equation 1 because they are not a primary source like joint torques or gravity but are a secondary source included in the motion-dependent effects arising from the primary sources.

The MDT plays a crucial role in the generation of angular accelerations that influence distal-point speed in high-speed swinging motions (Hirashima, 2008; Hirashima et al., 2008; Koike and Harada, 2014; Koike and Mimura, 2016a, 2016b; Naito and Maruyama, 2008; Naito et al., 2017; Putnam, 1991). Since the MDT is caused by product sums of angular velocities of individual segments, the MDT contribution will be relatively large when angular velocities of several segments increase before ball release or ball contact. The angular velocities of individual segments, caused by earlier joint torques, produce centrifugal and Coriolis forces, and thus the entire joint torque time-histories must be considered when investigating the MDT. At any given instant, previously applied joint torques can still exert an indirect effect on system behaviour through a mechanism sometimes called the "cumulative effect" of joint torque inputs (Zajac et al., 2003; Hirashima et al., 2008; Hirashima, 2008) or "whip-like effect" (Atwater, 1979; Feltner, 1989; Fleisig et al., 1996; Kibler, 1995; Kindall, 1992; Putnam, 1991). However, the contributions of these indirect effects to the generation of segmental speeds have not previously been quantified during any swinging motions. In place of quantifying these indirect effects of joint torque inputs, an analysis decomposing the MDT into kinematic sources (Hirashima et al., 2008; Naito et al., 2010; Naito et al., 2017) has been implemented to explain how the components generate speed. However, this analysis does not reveal which axis of each joint torque is crucial, or the time(s) at which a given joint torque is effective in contributing to the generation of a high distal-point speed. Greater understanding of how each joint torque contributes to speed generation through these indirect effects is still

needed. A conversion algorithm that quantifies the generating factors of the MDT has been introduced briefly (Koike and Harada, 2014), but without detailed methods, and was applied to high-speed swinging motions including the tennis serve (Koike and Harada, 2014), baseball batting (Koike and Mimura, 2016b), rugby place kicking (Koike and Bezodis, 2017), and baseball pitching (Koike, Uzawa and Hirayama, 2018). Although the factors contributing to the generation of the distal-point speed were examined for these motions, the direct and indirect effects of the joint torque inputs were not separately quantified.

The objectives of this study were to: (1) propose and describe a method which separately quantifies the direct and indirect effects of joint torques to the generation of distal-point speed in a multi-linked system; and (2) illustrate how the direct and indirect contributions differ in an example high-speed swinging motion: a rugby place kick.

2. Methods

2.1. Equation of motion for a multi-linked system

Since the equation of motion for a multi-linked system includes a cause-and-effect relationship between joint torque inputs and motion outputs, the general equation of motion (Equation 1) was used to derive a recurrence formula which can take the indirect effect of joint torque inputs into account. The proposed method was applied to the kicking-side lower limb segments during a rugby place kick.

The dynamical equation for the kicking-side leg, consisting of thigh, shank and foot segments, can be expressed as follows (see Appendix 1 for details):

$$\dot{\boldsymbol{V}} = \boldsymbol{A}_{\boldsymbol{V},\boldsymbol{T}_\mathrm{a}}\boldsymbol{T}_\mathrm{a} + \overline{\boldsymbol{A}}_{\boldsymbol{V},\mathrm{MDT}}(\boldsymbol{V})\boldsymbol{V} + \boldsymbol{A}_{\boldsymbol{V},\boldsymbol{G}}\boldsymbol{G} + \boldsymbol{B}_{\boldsymbol{V},\mathrm{other}} \tag{2}$$

where the vector $\boldsymbol{V}$ denotes the generalised velocity vector $\boldsymbol{V} = \left[\dot{\boldsymbol{x}}_1^\mathrm{T} \;\; \boldsymbol{\omega}_1^\mathrm{T} \;\; \dot{\boldsymbol{x}}_2^\mathrm{T} \;\; \boldsymbol{\omega}_2^\mathrm{T} \;\; \dot{\boldsymbol{x}}_3^\mathrm{T} \;\; \boldsymbol{\omega}_3^\mathrm{T}\right]^\mathrm{T}$, which consists of the

linear velocity vector $\dot{\boldsymbol{x}}_i$ and angular velocity vector $\boldsymbol{\omega}_i$ of all segments (where subscript *i* denotes segment number: *i*=1, thigh; *i*=2, shank; *i*=3, foot). The terms on the right-hand-side of Equation 2 represent the respective contributions to the generation of the generalised velocity vector of the joint torque term, motion-dependent term, gravitational term, and a term consisting of all the remaining sources with the matrices $\boldsymbol{A}_{\boldsymbol{V},\boldsymbol{Ta}}$ and $\boldsymbol{A}_{\boldsymbol{V},\boldsymbol{G}}$ indicating the coefficient matrices for the joint torque vector $\boldsymbol{T}_{\mathrm{a}}$ and gravitational force vector $\boldsymbol{G}$, $\bar{\boldsymbol{A}}_{\boldsymbol{V},\mathrm{MDT}}(\boldsymbol{V})$ being the coefficient matrix associated with the MDT and $\boldsymbol{B}_{\boldsymbol{V},\mathrm{other}}$ indicating the vector consisting of the remaining terms:

$$\boldsymbol{B}_{\boldsymbol{V},\mathrm{other}} = \boldsymbol{A}_{\boldsymbol{V},\mathrm{Hip}}\ddot{\boldsymbol{x}}_{\mathrm{Hip}} + \boldsymbol{A}_{\boldsymbol{V},\boldsymbol{\eta}}\ddot{\boldsymbol{\eta}} + \boldsymbol{A}_{\boldsymbol{V},\boldsymbol{\varphi}}\ddot{\boldsymbol{\varphi}} \tag{3}$$

where the matrix $\boldsymbol{A}_{\boldsymbol{V},\mathrm{Hip}}$ is the coefficient matrix for hip joint acceleration $\ddot{\boldsymbol{x}}_{\mathrm{Hip}}$, the matrices $\boldsymbol{A}_{\boldsymbol{V},\eta}$ and $\boldsymbol{A}_{\boldsymbol{V},\varphi}$ are coefficient matrices for the vectors $\ddot{\boldsymbol{\eta}}$ and $\ddot{\boldsymbol{\varphi}}$, respectively (see Appendix 1 for more detail). These three terms on the right-hand side correspond to the hip joint acceleration, segment length fluctuation and anatomical constraint joint axial angle fluctuation terms, respectively.

Similarly to the combination of "instantaneous and cumulative acceleration vectors" in previous studies (Hirashima et al., 2008; Zajac et al, 2003), the generalised acceleration vector $\dot{\boldsymbol{V}}$ can be expressed as the sum of two types of acceleration vector:

$$\dot{\boldsymbol{V}} = \dot{\boldsymbol{V}}_{\mathrm{Dir}} + \dot{\boldsymbol{V}}_{\mathrm{Indir}}, \tag{4}$$

where $\dot{\boldsymbol{V}}_{\mathrm{Dir}}$ denotes the acceleration vector due to the direct effect of joint torque, gravity and other inputs:

$$\dot{\boldsymbol{V}}_{\mathrm{Dir}} = \boldsymbol{A}_{\boldsymbol{V},\boldsymbol{T}\mathrm{a}}\boldsymbol{T}_{\mathrm{a}} + \boldsymbol{A}_{\boldsymbol{V},\boldsymbol{G}}\boldsymbol{G} + \boldsymbol{B}_{\boldsymbol{V},\mathrm{other}}, \tag{5}$$

and $\dot{\boldsymbol{V}}_{\mathrm{Indir}}$ denotes the acceleration vector due to the indirect effect of these inputs, mediated through motion-dependent processes arising from earlier direct effects:

$$\dot{\boldsymbol{V}}_{\mathrm{Indir}} = \bar{\boldsymbol{A}}_{\boldsymbol{V},\mathrm{MDT}}(\boldsymbol{V})\boldsymbol{V} \tag{6}$$

These relationships, expressed for a continuous-time system, can be represented with a block diagram (Figure 1).

** Figure 1 near here **

2.2. Derivation of a recurrence formula with respect to the generalised velocity vector

The generalised acceleration vector can be expressed by difference approximation using the time interval Δt of the discrete-time system shown as:

$$\dot{\boldsymbol{V}}(k) = \frac{\boldsymbol{V}(k+1) - \boldsymbol{V}(k)}{\Delta t} \tag{7}$$

After discretising Equations 4 to 6, combining Equations 4 to 7 yields a recurrence formula for the generalised velocity vector $\boldsymbol{V}$ as follows:

$$\boldsymbol{V}(k+1) = \Delta t \dot{\boldsymbol{V}}_{\mathrm{Dir}}(k) + \boldsymbol{\Psi}_{\boldsymbol{V}}(k)\boldsymbol{V}(k), \qquad \boldsymbol{\Psi}_{\boldsymbol{V}}(k) = \boldsymbol{E}_{18} + \Delta t \bar{\boldsymbol{A}}_{\boldsymbol{V},\mathrm{MDT}}(\boldsymbol{V}(k)) \tag{8}$$

where $\boldsymbol{E}_{18}$ is the unit matrix with eighteen rows and columns.

Since the coefficient matrix $\bar{\boldsymbol{A}}_{\boldsymbol{V},\mathrm{MDT}}(\boldsymbol{V}(k))$ contains the angular velocity of the generalised velocity vector $\boldsymbol{V}(k)$ in its elements, the coefficient matrix $\boldsymbol{\Psi}_{\boldsymbol{V}}(k)$ also contains the elements $\boldsymbol{V}(k)$. Although it is possible to numerically obtain the states of the individual segments (e.g. linear and angular velocity vectors) for the individual input terms using discretised Equations 5, 6 and 8, it would be impossible to calculate the indirect effect of the input terms using these equations because Equation 8 is not a form of primary expression with respect to the vector $\boldsymbol{V}(k)$.

Thus, in order to quantify the indirect effect of the individual input terms, the generalised velocity vector $\boldsymbol{V}(k)$ in the matrix $\bar{\boldsymbol{A}}_{\boldsymbol{V},\mathrm{MDT}}(\boldsymbol{V}(k))$ in Equation 8 must be replaced with the generalised velocity vector $\tilde{\boldsymbol{V}}(k)$ measured at the k-th time instant:

$$\boldsymbol{V}(k+1) = \Delta t \dot{\boldsymbol{V}}_{\mathrm{Dir}}(k) + \tilde{\boldsymbol{\Psi}}_{\boldsymbol{V}}(k)\boldsymbol{V}(k), \qquad \tilde{\boldsymbol{\Psi}}_{\boldsymbol{V}}(k) = \boldsymbol{E}_{18} + \Delta t \bar{\boldsymbol{A}}_{\boldsymbol{V},\mathrm{MDT}}(\tilde{\boldsymbol{V}}(k)) \tag{9}$$

Since the vector $\widetilde{\boldsymbol{\Psi}}_{\boldsymbol{V}}(k)\boldsymbol{V}(k)$ has a form of primary expression with respect to the velocity vector $\boldsymbol{V}(k)$, the recurrence formula, Equation 9, can be expressed from the beginning of the motion to the k-th time instant of analysis (Figure 2a), and reshaped as shown in Figure 2b, where it becomes possible to quantify the total effect (i.e. direct and indirect effects) of individual torque inputs to the generation of the generalised velocity vector.

Equations 5 and 9 can quantify the contributions of the individual input terms (i.e. the joint torque term, the gravitational term, the hip-joint acceleration term, the segment length fluctuation term, and the anatomical constraint joint axial angle fluctuation term) at time k to the generation of the generalised velocity vector at time k+1 considering the generating factors of the MDT.

** Figure 2 near here **

The total effects of joint torque inputs on the generation of the foot centre of gravity (CG) speed are expressed by a block diagram (Figure 3a) consisting of the direct effect component (Figure 3b) and indirect effect component (Figure 3c).

** Figure 3 near here **

The direct and indirect effects of the individual joint torque inputs in generating the MDT can be quantified from Figure 3 (see Appendix 2 for details). The MDT contribution can be decomposed into kinematic components arising from centrifugal forces, Coriolis forces, gyroscopic effect moments and segmental length fluctuations (see Appendix 3 for details).

2.3. Data collection

Six male rugby players (two professional and four university-level; mean ± SD of age: 21.9±1.8 years; height: 1.77±0.06 m; body mass: 81.8±4.4 kg) performed 5 - 8 place kicks. Each provided written informed consent, and study approval was obtained from the lead author's institution's ethics committee. The ball was placed on their preferred tee and kicked into a net approximately 4 m away. The kickers were instructed to kick as far and as straight (towards the centre of the net) as possible. Kinematic data (47 markers on the body, 6 on the ball) were recorded with a 14-camera motion capture system (VICON-MX, Vicon Motion Systems Ltd., Oxford, UK; 500 Hz). Kinetic data under the support leg were measured with a force platform (9287C, Kistler Inst.; 1000Hz). The kicking action was divided into two phases: flight and support. These were, respectively, the period from the final take-off of the kicking foot (KFO) to ground contact with the support foot (SFC), and the period from SFC to ball contact (BC). KFO was defined as when the kicking foot's 5^{th} MTP marker first reached a vertical displacement of 0.10 m after its final ground contact prior to ball contact (Lees et al., 2009); SFC was based on a vertical ground reaction force threshold of

10 N, and BC was defined as the frame of peak anterior toe velocity (Shinkai et al., 2009). All data were time-normalised to phase durations as -200% to -100% (flight, KFO to SFC) and -100% to 0% (support, SFC to BC). Anatomical constraint axes (e.g. varus-valgus axis at knee joint; internal-external rotation axis at ankle joint) were also considered in the modelling (Koike et al., 2017). The coordinate data were smoothed with a fourth-order zero-phase-shift Butterworth low-pass digital filter whose optimal cut-off frequencies (5 - 15 Hz) were determined by residual analysis (Wells and Winter, 1980). Three trials per participant were selected based on the participants' highest subjective ratings, and the mean data across these trials were used for each participant.

3. Results

The flight and support phases lasted 0.11±0.01 and 0.13±0.01 seconds, respectively. The directly measured kicking foot CG speed gradually increased until -60% (normalised) time, then increased rapidly toward BC, reaching 21.34±0.70 m/s at BC (Figure 4a). The sum of the MDT and the contributions induced by the direct effect of individual terms matched the measured foot CG's speed to within 0.19 m/s throughout the movement (Figures 4a to h). Similarly, the total of the contributions induced by both the direct and indirect effects of individual terms, following the partition of the MDT into its component indirect terms, also matched the measured foot CG's speed to within 0.14 m/s (Figures 4a, c to h).

The MDT was the dominant contributor to the foot CG's speed. The centrifugal force component accounted for most of this MDT contribution (Figure 4b), but the Coriolis force component was also appreciable during the support phase; the components relating to the gyroscopic effect moment and the segment length fluctuations were very small throughout. The MDT's dynamic contribution increased gradually toward -95% time, then decreased until -50%,

before increasing rapidly toward BC where it reached 20.84±3.67 m/s, or 98% of the foot CG's speed at this instant (Figure 4b). After partitioning the MDT into its components, the total contribution from the direct effects of the individual joint torque inputs increased until -35% time and then decreased toward BC, while the total indirect effects of these inputs increased after -60% time toward BC (Figure 4c). The direct effect of the initial velocity term was positive until -120% time and then became negative toward BC, whereas the indirect effect of the velocity term was positive throughout, increasing until -90% time and then decreasing toward BC (Figure 4d). The contributions from the direct and indirect effects of the gravitational force term, the hip joint acceleration term, the segment length fluctuation term and the joint anatomical constraint axes fluctuation term were small (Figure 4e-h).

Consideration of the time derivatives of the direct and indirect effects associated with the torques for individual joint rotations allows identification of the times when, and the specific axes about which, key contributions to the kicking foot CG's speed at BC ($s_3(k_{\mathrm{BC}})$; Figure 5) occurred. Peak positive contributions from the direct and indirect effects of the hip flexion-extension torque occurred around -110 and -90% time, respectively (Figure 5a). The indirect contributions from knee flexion-extension and ankle plantar-dorsiflexion torques were also positive (Figure 5d and f) but these peaked slightly later (around -70% time). At this time, the direct effects of these knee and ankle torques were large and negative (Figure 5d and f). Aside from the indirect effect of the ankle eversion-inversion torque, particularly after SFC, the other non-sagittal plane torques made only small contributions throughout the entire movement (Figure 5b, c, e and g).

The integrated contribution across each phase to the foot CG's speed at BC was also determined for both the direct and indirect effects of each individual axial torque (Figure 6a and b). The direct and indirect effects of the hip flexion-extension torque contributed positively to the foot CG's speed at BC across both the flight phase and the

subsequent support phase. The indirect effects of the ankle plantar-dorsal flexion torques and the direct effects of the knee flexion-extension torques, both across the support phase, showed the largest positive and negative contributions, respectively.

** Figure 4 near here **

** Figure 5 near here **

** Figure 6 near here **

4. Discussion

This study firstly aimed to propose and describe a method which separately quantifies the direct and indirect effects of joint torque inputs in the distal-point speed generation of a high-speed swinging motion. Secondly, we aimed to illustrate how the model outputs differ between these direct and indirect effects, using a rugby place kick as an example motion. The indirect effects of the joint torques, which are generated through motion-dependent processes as a result of previously-exerted joint torques, were the largest contributor to the foot CG's speed at BC in this rugby kicking motion (Figure 4c). Although the overall sum of the direct effects of joint torques showed only a small contribution to the foot CG's speed at BC (Figure 4c), the direct effect of the hip flexion-extension torque (flexor dominant throughout) was the major positive contributor to the foot CG's speed at BC, and this contributed during both flight and support (Figures 6a and b). Interestingly, the indirect effects of the knee flexion-extension torque (extensor dominant until -20%, then flexor dominant) and ankle plantar-dorsal flexion torque (dorsiflexor dominant throughout) showed positive contributions, whereas the direct effects of those torques contributed negatively (Figures 5d and f, Figures 6a and b). Although exerting a knee extension torque would induce knee extension and therefore contribute geometrically to the foot CG's speed, a negative direct contribution of knee extension torque to the foot

CG's speed was observed in this study. This non-intuitive phenomenon may be caused by the dynamic coupling (Kane and Levinson, 1985) of the leg segments in which the knee extension torque would induce extension of hip joint, and this hip extension would reduce the foot CG's speed, where dynamic coupling means that a torque input about one joint axis can cause multi-axial angular accelerations of the body due to the non-diagonal inertial matrix of the equation of motion for the system (Hirashima et al., 2007, 2008; Koike et al., 2017; Zajac et al., 2002, 2003). Further investigation, using an induced joint angular velocity analysis, would be needed to verify this explanation. Since a flexion torque was exerted about the hip joint throughout the movement and contributed positively to the foot CG's speed via both direct and indirect effects, torque reversal – as found to be effective in Herring and Chapman's (1992) simulation of a throwing motion – was not observed in this kicking motion. The relatively small effects of the hip joint torques about the other axes (Figure 5b and 5c) support previous kinematic data which suggested that the contributions of the hip adduction-abduction and internal-external rotation angular velocities to foot speed in rugby place kicking are small (Zhang et al., 2012). Finally, the large contribution of the indirect effect of ankle plantar-dorsiflexion torques to the foot CG's speed (Figures 5f and 6b) may be because the foot is swung with high speed around the shank and thigh segments, and therefore this torque assists in effective orientation of the foot segment. This would help to control the impact location between the foot and ball, which is an important feature for determining the ball flight characteristics (Peacock and Ball, 2017). A similar effect was also evident in the ankle eversion-inversion torque (Figure 5g and Figure 6b).

The method proposed in this study quantifies both the direct and indirect effects of individual joint torque inputs in the generation of distal-point speed, and their use for evaluating performance, whereas previous studies showed only the direct effect of joint torques in actions such as the generation of elbow extension angular velocity (Hirashima

et al., 2008; Naito and Maruyama, 2008), of distal-point speed (Naito et al., 2017), and of angular velocities about the longitudinal axes of the upper arm and forearm segments (Naito et al., 2014) during overarm throwing and baseball pitching, and in the generation of knee extension angular velocity during soccer kicking motion (Naito et al., 2010). Although previous studies decompose the MDT into several components in order to describe how particular kinematic features of segmental and joint movements affect the MDT contributions (e.g. Hirashima et al., 2008; Naito and Maruyama, 2008; Naito et al., 2010; Naito et al., 2017; Putnam, 1991, 1993), kinematic analyses alone cannot reveal the mechanisms by which these movements induce effective joint torques.

The capability of the algorithm to calculate the direct and indirect effects separately during the analysis of high-speed swinging motions has been demonstrated. This approach can aid in the understanding of the specific effects of individual joint torques exerted during swinging motions. For example, in rugby place kicking, high foot speed at BC is required to achieve high ball launch velocities. In our analysis of the rugby place kick, the hip flexion-extension torque exerted at around -110% time caused large foot CG speed at BC via the direct effect of the torque, and the same axial torque exerted at around -90% time induced large foot CG speed at BC via the indirect effect. Since the foot CG's speed induced solely by the direct effect of joint torques is limited by the force-producing capacity of muscles crossing the joint, utilisation of the motion-dependent mechanisms is an effective strategy for producing higher distal-point speeds during such a high-speed motion. Because the indirect effect of the hip flexion-extension torque exerted around -90% time plays a significant role in the speed generation of the foot's CG at BC by enhancing the contributions of the MDT prior to BC (Figures 5a and 6b), it is necessary to examine the direct and indirect effects separately. The indirect effects of the knee flexion-extension and ankle plantar-dorsiflexion torques peaked after the indirect effect of the hip flexion-extension torque, and the timing of these peaks (at approximately

-70% time) occurred close to where the centrifugal and Coriolis force components of the MDT inflected (Figure 4b). While the ankle joint torque also plays a role via the indirect effect in the foot CG's speed generating mechanism (Figure 5f), the role of the knee joint extension-flexion torque via the direct effect would be to prevent knee-joint hyperextension (Apriantono et al., 2006; Dörge et al., 2002) and the role of the ankle plantar-dorsiflexion torque via the direct effect may be to control the foot for accurate contact with the ball.

This study has presented the contributions to the kicking foot CG's speed using a model consisting only of the kicking-side thigh, shank and foot segments. Since the current model consists of only these segments, the contributions of joint torques other than the kicking-leg joint torques were not quantified. Thus, an analysis using a whole-body model would be necessary to fully clarify the roles of all joint torques during rugby place kicking. A more complete investigation of the whole-body kicking motion would require investigation of the contributions to the angular velocities such as joint angular velocities and foot angular velocity using a whole-body model. However, focusing on just the kicking leg is an appropriate starting point in understanding such complex high-speed swinging motions, particularly given the primary aim of our study was to detail the model and demonstrate its potential. This method can now be applied to any swinging motion, in a whole-body or part-body way, for a more complete understanding of the distal-point speed generating mechanisms. Since this approach enables the effects of joint torque inputs to be obtained even when the MDT plays a crucial role in the distal-point speed generation, estimation of muscle force contributions can be performed by solving the load distribution problem with use of musculoskeletal models (e.g. Delp et al., 2007).

5. Conclusion

A method for quantifying direct and indirect effects of joint torque inputs in the speed generating mechanism of a swinging motion has been introduced, in which a direct effect is generated by angular accelerations induced by a joint torque at a given instant, whereas an indirect effect is generated through a motion-dependent term (MDT: a nonlinear term consisting of centrifugal force, Coriolis force and a gyroscopic effect moment) induced by earlier application of a joint torque. The method allows identification of the individual joint torque axes and timings of joint torque exertion that are used to generate a high speed of the distal point of a multi-linked system. The two types of effect were quantified for joint torque inputs through a recurrence formula with respect to the generalised velocity vector of a multi-linked system based on the equation of the system's motion including a cause-and-effect relationship between joint torque inputs and motion outputs. The practical potential of this approach has been demonstrated through its application to modelling the role of the kicking-side leg in generating foot speed during a rugby place kick. Important contributions to foot CG speed, for example from the direct and indirect effects of the hip flexion-extension torque during the flight phase and the subsequent support phase, were identified by considering the factors responsible for generating the MDT. Further investigation will be needed to determine both direct and indirect effects for whole-body joint torque inputs in the generation of distal-point speed in swinging motions.

Acknowledgements

This work was partly supported by The Great Britain Sasakawa Foundation [grant numbers 5029 (Bezodis) and 5226 (Willmott)] which had no involvement in the study design, study execution, the writing of the manuscript, or the decision to submit it for publication. The authors thank Naoki Numazu for his assistance with data collection and processing.

Conflict of interest

The authors declare no conflicts of interest to report in this research.

References

Apriantono, T., Nunome, H., Ikegami, Y., Sano, S., 2006. The effect of muscle fatigue on instep kicking kinetics and kinematics in association football. Journal of Sports Sciences. 24, 951-960.

Atwater, A.E., 1979. Biomechanics of overarm throwing movements and of throwing injuries. Exercise and Sport Sciences Reviews 7, 43-85.

Delp, S. L., Anderson, F. C., Arnold, A. S., Loan, P., Habib, A., John, C. T., Thelen, D. G., 2007. OpenSim: open-source software to create and analyze dynamic simulations of movement. IEEE Transactions on Biomedical Engineering 54, 1940-1950.

Dörge, H. C., Bullandersen, T, Sorensen, H., Simonsen, E. B. 2002. Biomechanical differences in soccer kicking with the preferred and the non-preferred leg. Journal of Sports Sciences. 20, 293-299.

Elliott, B., Fleisig, G., Nicholls, R., Escamilia, R., 2003. Technique effects on upper limb loading in the tennis serve. Journal of Science and Medicine in Sport 6, 76–87.

Feltner, M., Dapena, J., 1986. Dynamics of the shoulder and elbow joints of the throwing arm during a baseball pitch. International Journal of Sport Biomechanics 2, 235-259.

Feltner, M.E., 1989. 3-dimensional interactions in a 2-segment kinetic chain. Part II: Application to the throwing arm in baseball pitching. International Journal of Sport Biomechanics 5, 420–450.

Fleisig, G.S., Andrews, J.R., Dillman, C.J., Escamilla, R.F., 1995. Kinetics of baseball pitching with implications about injury mechanisms. American Journal of Sports Medicine 23, 233-239.

Fleisig, G.S., Barrentine, S.W., Escamilla, R.F., Andrews, J.R., 1996a. Biomechanics of overhand throwing with implications for injuries. Sports Medicine 21, 421-437.

Fleisig, G.S., Escamilla, R.F., Andrews, J.R., Matsuo, T., Satterwhite, Y., Barrentine, S.W., 1996b. Kinematic and kinetic comparison between baseball pitching and football passing. Journal of Applied Biomechanics 12, 207-224.

Herring, R.M., Chapman, A.E., 1992. Effects of changes in segmental values and timing of both torque reversal in simulated throws. Journal of Biomechanics 25, 1173-1184.

Hirashima, M., 2008. Induced acceleration analysis of three-dimensional multi-joint movements and its application to sports movements. Theoretical Biomechanics, edited Vaclav Klika, InTech.

Hirashima, M., Kudo, K., Ohtsuki, T., 2007. A new non-orthogonal decomposition method to determine effective torques for three-dimensional joint rotation. Journal of Biomechanics 40, 871-882.

Hirashima, M., Yamane, K., Nakamura, Y., Ohtsuki, T., 2008. Kinetic chain of overarm throwing in terms of joint rotations revealed by induced acceleration analysis. Journal of Biomechanics 41, 2874-2883.

Kane, T. R., Levinson D. A., 1985. Dynamics: Theory and Applications. McGraw-Hill, New York, USA.

Kepple, T.M.; Siegel, K.L. Stanhope, S.J., 1997. Relative contributions of the lower extremity joint moments to forward progression and support during gait. Gait and Posture 6, 1-8.

Kibler, W.B., 1995. Biomechanical analysis of the shoulder during tennis activities. Clinics in Sports Medicine 14, 79-85.

Kindall, J., 1992. Science of coaching baseball. Human Kinetics Publishers.

Koike, S., Bezodis, N., 2017. Determining the dynamic contributions to kicking foot speed in rugby place kicking. In Proceedings of the 35th International Conference on Biomechanics in Sports, German Sport University Cologne, Cologne.

Koike, S., Harada, Y., 2014. Dynamic Contribution Analysis of Tennis-serve-motion in Consideration of Torque Generating Mode, Procedia Engineering 72, 97–102.

Koike, S., Mimura, K., 2016a. Contributions of joint torques, motion-dependent term and gravity to the generation of baseball bat head speed. Procedia Engineering 147, 191-196.

Koike, S., Mimura, K., 2016b. Main contributors to the baseball bat head speed considering the generating factor of motion-dependent term. Procedia Engineering 147, 197-202.

Koike, S., Nakaya, S., Mori, H., Ishikawa, T., Willmott, A.P., 2017. Modelling error distribution in the ground reaction force during an induced-acceleration analysis of running in rear-foot strikers. Journal of Sports Sciences, (Published online).

Koike, S., Uzawa, H., Hirayama, D., 2018. Generation mechanism of linear and angular ball velocity in baseball pitching. Proceedings 2018, 2, 206.

Lees, A., Rahnama, N., 2013. Variability and typical error in the kinematics and kinetics of the maximal instep kick in soccer. Sports Biomechanics 12, 283–292.

Naito, K., Fukui, Y., Maruyama, T., 2010. Multijoint kinetic chain analysis of knee extension during the soccer instep kick. Human Movement Science 29, 259-276.

Naito, K., Maruyama, T., 2008. Contributions of the muscular torques and motion-dependent torques to generate rapid

elbow extension during overhand baseball pitching. Sports Engineering 11, 47-56.

Naito, K., Takagi, T., Kubota, H., Maruyama, T., 2017. Multi-body dynamic coupling mechanism for generating throwing arm velocity during baseball pitching. Human Movement Science 54, 363-376.

Naito, K., Takagi, H., Yamada, N., Hashimoto, S., Maruyama, T., 2014. Intersegmental dynamics of 3D upper arm and forearm longitudinal axis rotations during baseball pitching. Human Movement Science 38, 116-132.

Nunome, H., Asai, T., Ikegami, Y., Sakurai, S., 2002. Three-dimensional kinetic analysis of side-foot and instep soccer kicks. Medicine and Science in Sports and Exercise 34, 2028-2036.

Peacock, J.C.A., Ball, K., 2017. The relationship between foot-ball impact and flight characteristics in punt kicking. Sports Engineering 20, 221-230.

Putnam, C.A., 1991. A segment interaction analysis of proximal-to-distal sequential segment motion patterns. Medicine and Sciences in Sports and Exercise 23, 130-144.

Putnam, C.A., 1993. Sequential motions of body segments in striking and throwing skills: Descriptions and explanations. Journal of Biomechanics 26, 125-135.

Reid M., Elliott B., Alderson J., 2007. Shoulder joint loading in the high performance flat and kick tennis serves. British Journal of Sports Medicine 41, 884–889.

Shinkai, H., Nunome, H., Isokawa, M., Ikegami, Y., 2009. Ball impact dynamics of instep soccer kicking. Medicine and Science in Sports and Exercise 41, 889-897.

Zajac, F.E., Neptune, R.R., Kautz, S.A., 2002. Biomechanics and muscle coordination of human walking. Part I: introduction to concepts, power, transfer, dynamics and simulations. Gait and Posture 16, 215-232.

Zajac, F.E., Neptune, R.R., Kautz, S.A., 2003. Biomechanics and muscle coordination of human walking. Part II:

lessons from dynamical simulations and clinical applications. Gait and Posture 17, 1-17.

Zhang, Y., Liu, G., Xie, S., 2012. Movement sequences during instep rugby kick: a 3D biomechanical analysis. International Journal of Sports Science and Engineering, 6, 89-95.

Figure

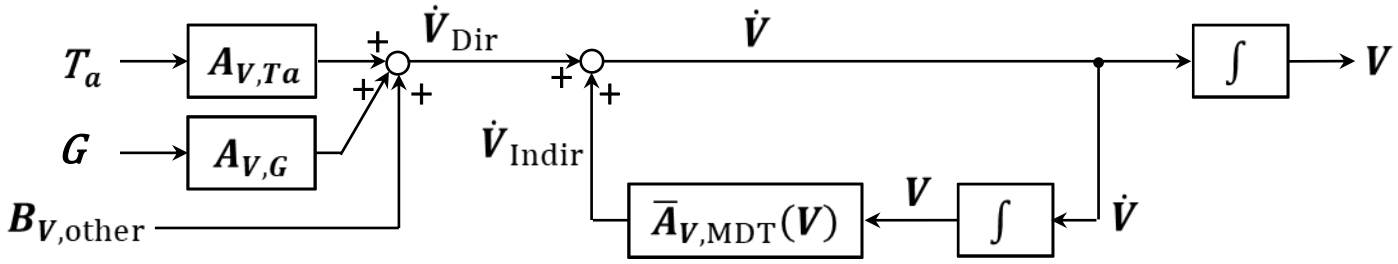

Figure 1

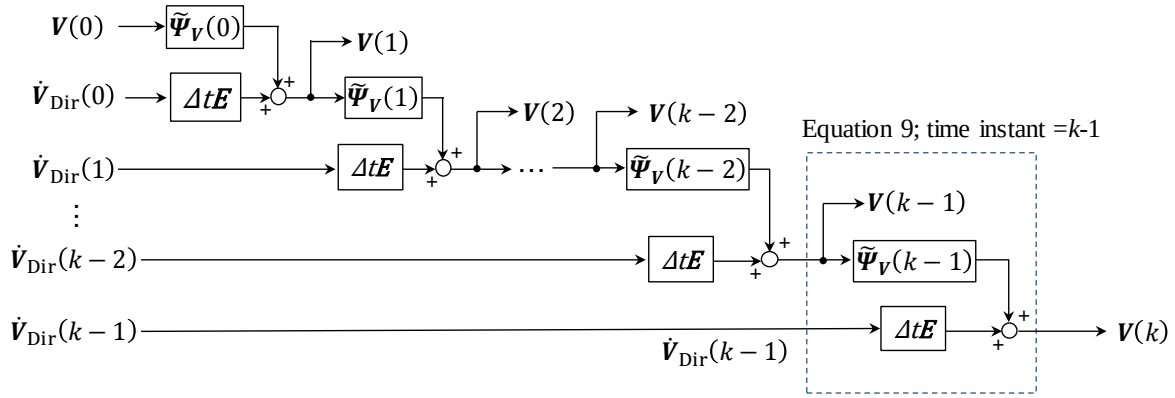

(a). A block diagram representing the recurrence formula with respect to the generalised velocity vector.

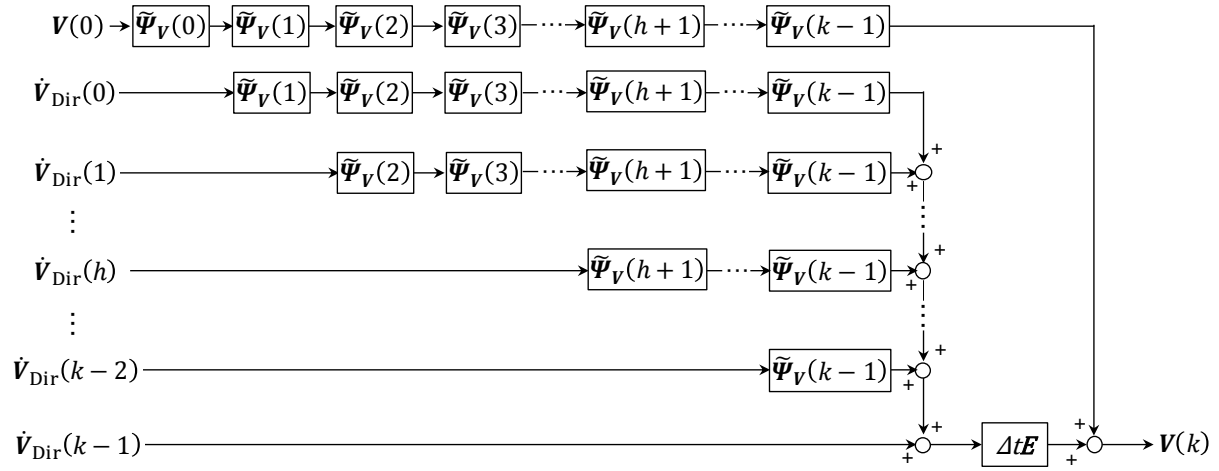

(b). A reshaped block diagram representing the recurrence formula with respect to the generalised velocity vector.

Figure 2

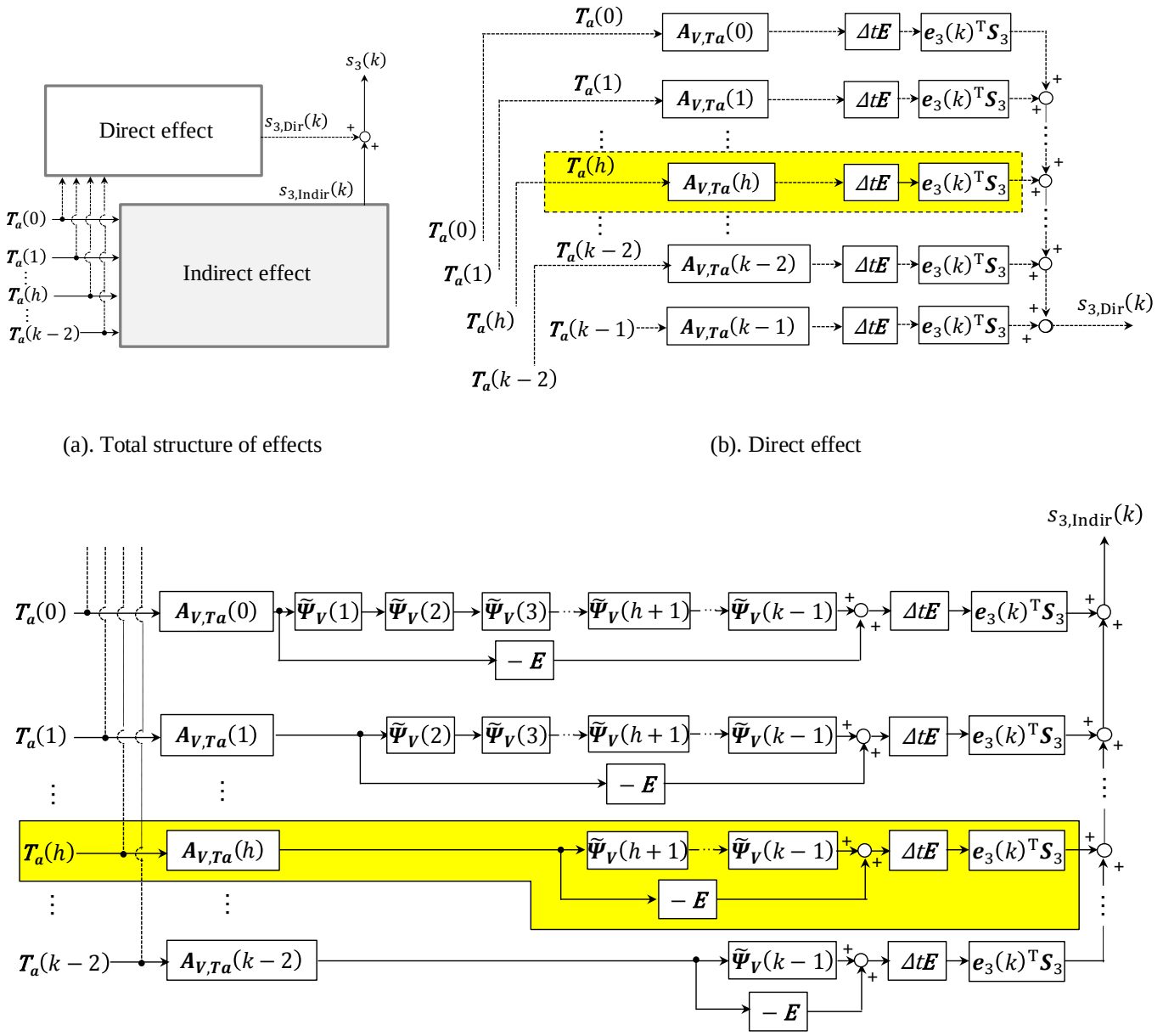

(a). Total structure of effects

(b). Direct effect

(c). Indirect effect

Figure 3

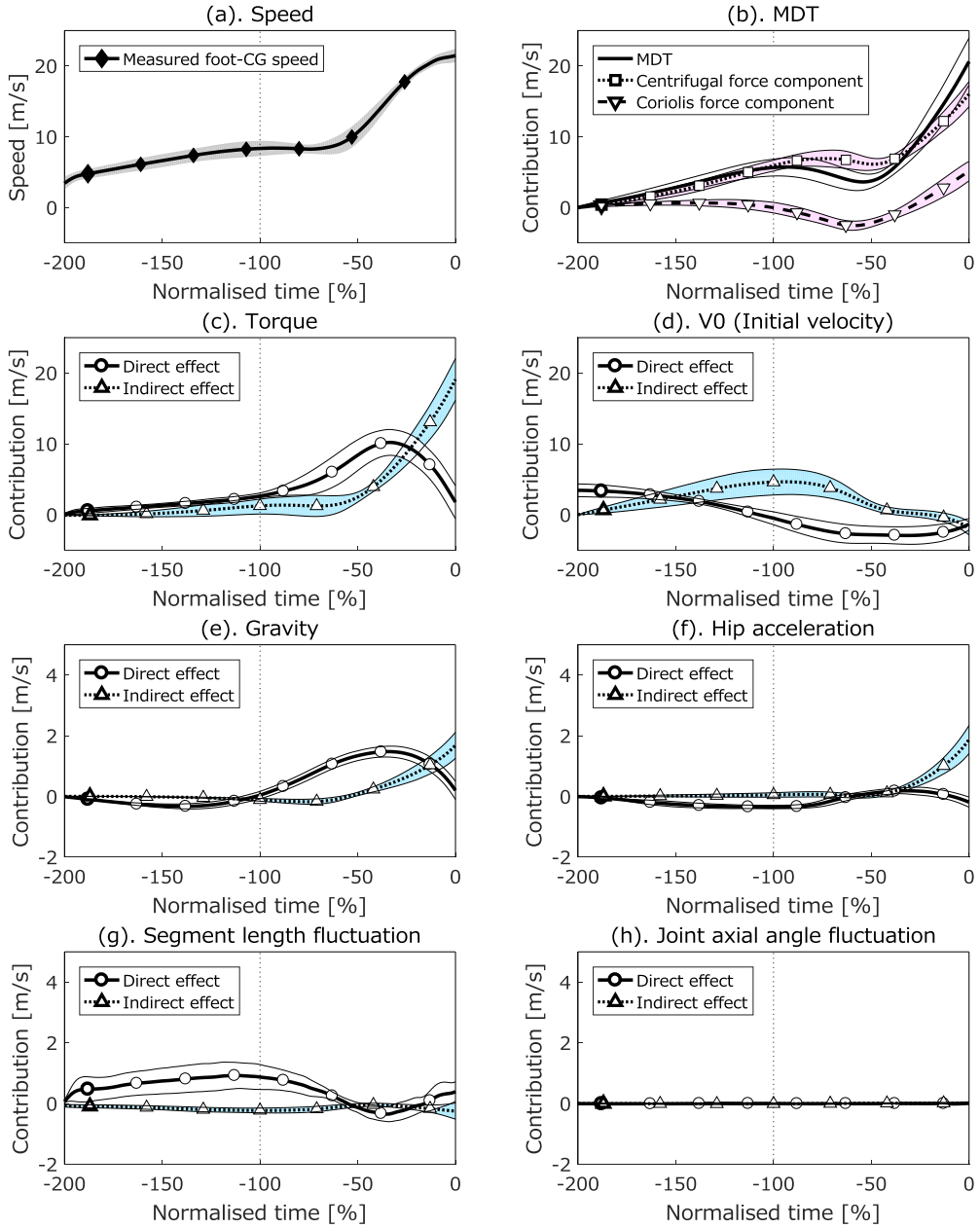
(a). Speed
Measured foot-CG speed
Speed [m/s]
Normalised time [%]
(b). MDT
MDT
Centrifugal force component
Coriolis force component
Contribution [m/s]
Normalised time [%]
(c). Torque
Direct effect
Indirect effect
Contribution [m/s]
Normalised time [%]
(d). V0 (Initial velocity)
Direct effect
Indirect effect
Contribution [m/s]
Normalised time [%]
(e). Gravity
Direct effect
Indirect effect
Contribution [m/s]
Normalised time [%]
(f). Hip acceleration
Direct effect
Indirect effect
Contribution [m/s]
Normalised time [%]
(g). Segment length fluctuation
Direct effect
Indirect effect
Contribution [m/s]
Normalised time [%]
(h). Joint axial angle fluctuation
Direct effect
Indirect effect
Contribution [m/s]
Normalised time [%]

Figure 4

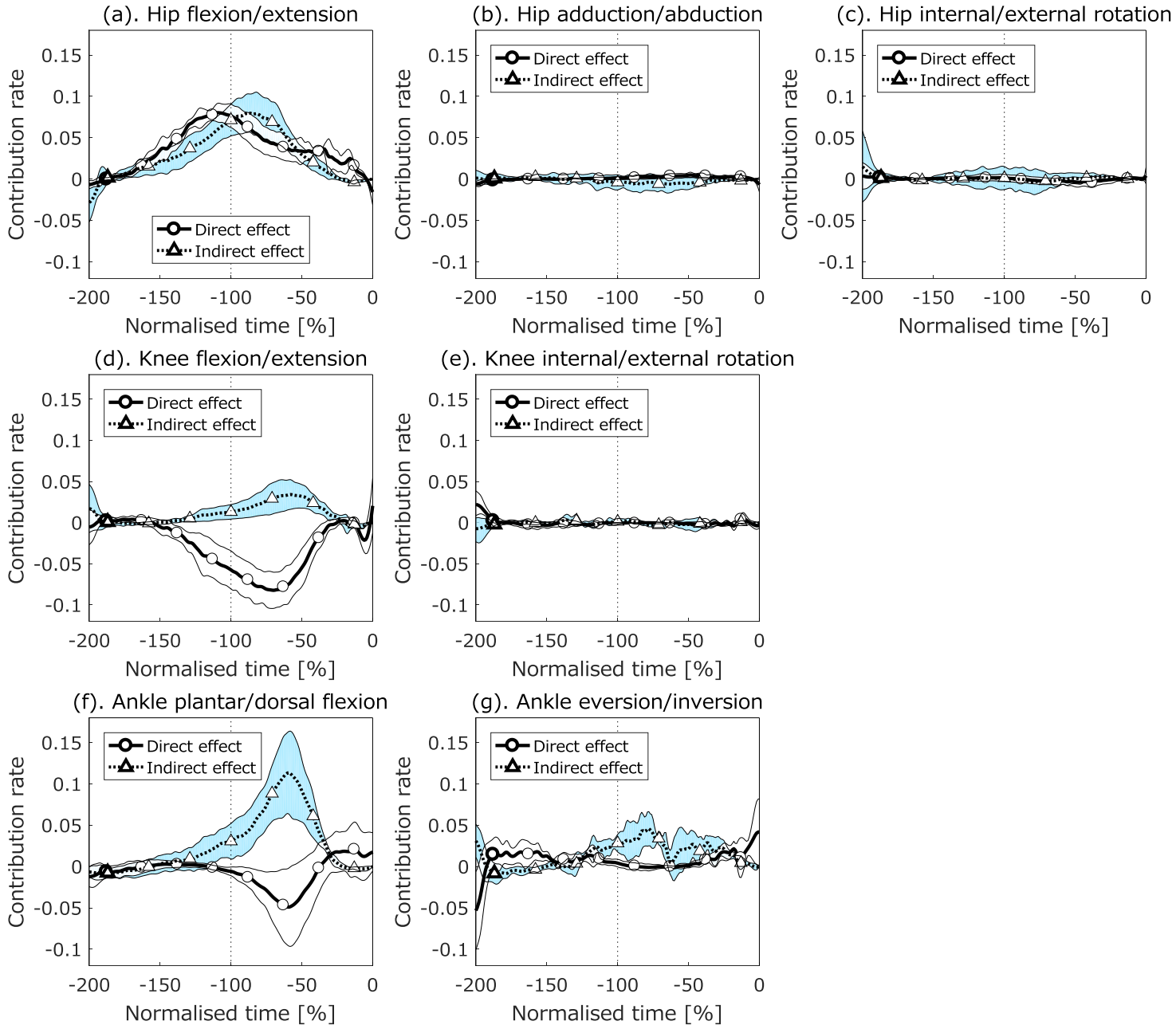
(a). Hip flexion/extension
(b). Hip adduction/abduction
(c). Hip internal/external rotation
(d). Knee flexion/extension
(e). Knee internal/external rotation
(f). Ankle plantar/dorsal flexion
(g). Ankle eversion/inversion
Contribution rate
Normalised time [%]
Direct effect
Indirect effect
0.15
0.1
0.05
0
-0.05
-0.1
-200
-150
-100
-50
0

Figure 5

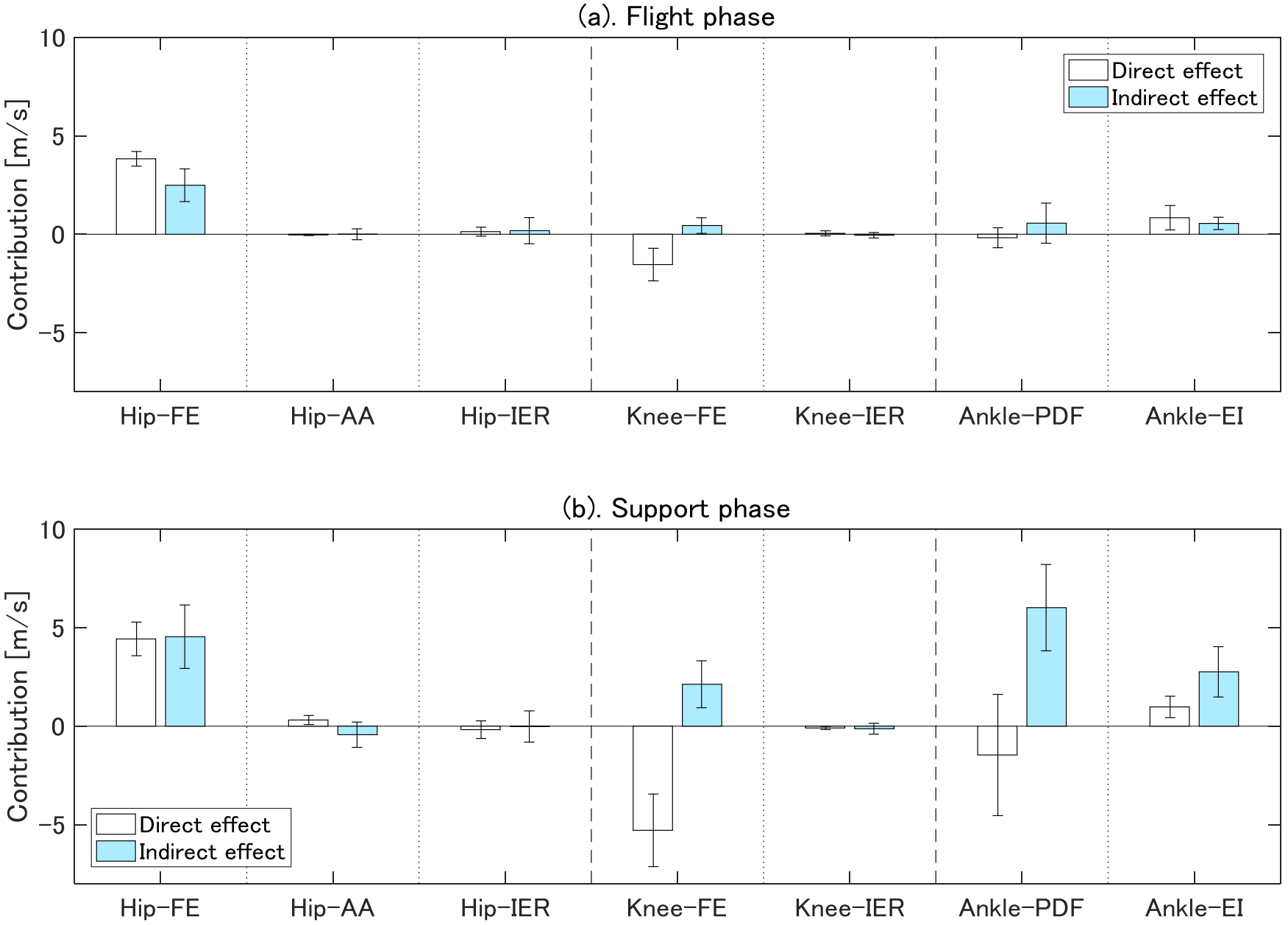
(a). Flight phase
Contribution [m/s]
10
5
0
−5
Direct effect
Indirect effect
Hip−FE
Hip−AA
Hip−IER
Knee−FE
Knee−IER
Ankle−PDF
Ankle−EI
(b). Support phase
Contribution [m/s]
10
5
0
−5
Direct effect
Indirect effect
Hip−FE
Hip−AA
Hip−IER
Knee−FE
Knee−IER
Ankle−PDF
Ankle−EI

Figure 6

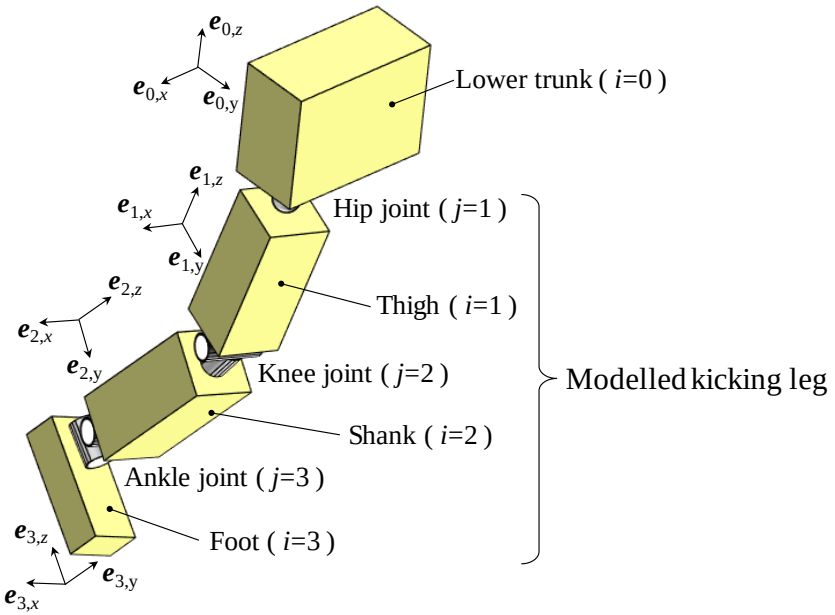
$e_{0,z}$
$e_{0,x}$
$e_{0,y}$
Lower trunk (i=0)
$e_{1,z}$
$e_{1,x}$
$e_{1,y}$
Hip joint (j=1)
Thigh (i=1)
$e_{2,z}$
$e_{2,x}$
$e_{2,y}$
Knee joint (j=2)
Shank (i=2)
Ankle joint (j=3)
Foot (i=3)
$e_{3,z}$
$e_{3,y}$
$e_{3,x}$
Modelled kicking leg

Figure A1

Appendices

Appendix 1

Figure A1 shows a schematic diagram of a kicking-leg model containing three rigid segments – the thigh, shank and foot – with the lower trunk segment also described but not included in the model. Under the assumption that the human body can be modelled as a multi-linked system of rigid segments, the dynamical equations for individual segments can be expressed in a matrix form with respect to all segments as follows (Koike et al., 2017):

$$\boldsymbol{M}\dot{\boldsymbol{V}} = \boldsymbol{P}\boldsymbol{F} + \boldsymbol{Q}\boldsymbol{N} + \boldsymbol{H} + \boldsymbol{G} \tag{A1}$$

where $\boldsymbol{M}$ is the inertia matrix, and $\boldsymbol{V}$ is the generalised velocity vector consisting of linear velocity vectors and angular velocity vectors for all the segments. $\boldsymbol{P}$ is the coefficient matrix for vector $\boldsymbol{F}$ which contains all joint force vectors. $\boldsymbol{Q}$ is the coefficient matrix for vector $\boldsymbol{N}$ which contains all joint moment vectors. $\boldsymbol{H}$ is the gyroscopic effect moment vector, and $\boldsymbol{G}$ is the vector due to the gravitational force.

Details of the matrices identified in the dynamical equations in Equation A1 are as follows: matrices $\boldsymbol{O}$ and $\boldsymbol{E}$, without a subscript, denote the zero and unit matrices with three rows and three columns, and matrix $\boldsymbol{O}$ with a subscript *mxn* denotes the zero matrix with *m* rows and *n* columns.

$$\boldsymbol{V} = \left[\dot{\boldsymbol{x}}_1^{\mathrm{T}} \;\; \boldsymbol{\omega}_1^{\mathrm{T}} \;\; \dot{\boldsymbol{x}}_2^{\mathrm{T}} \;\; \boldsymbol{\omega}_2^{\mathrm{T}} \;\; \dot{\boldsymbol{x}}_3^{\mathrm{T}} \;\; \boldsymbol{\omega}_3^{\mathrm{T}}\right]^{\mathrm{T}}, \boldsymbol{F} = \left[\boldsymbol{f}_1^{\mathrm{T}} \;\; \boldsymbol{f}_2^{\mathrm{T}} \;\; \boldsymbol{f}_3^{\mathrm{T}}\right]^{\mathrm{T}}, \boldsymbol{N} = \left[\boldsymbol{n}_1^{\mathrm{T}} \;\; \boldsymbol{n}_2^{\mathrm{T}} \;\; \boldsymbol{n}_3^{\mathrm{T}}\right]^{\mathrm{T}} \tag{A2}$$

$$\boldsymbol{M} = \text{block diag}\{m_1\boldsymbol{E}, \hat{\boldsymbol{I}}_1, m_2\boldsymbol{E}, \hat{\boldsymbol{I}}_2, m_3\boldsymbol{E}, \hat{\boldsymbol{I}}_3\} \tag{A3}$$

$$\boldsymbol{P}=\begin{bmatrix} \boldsymbol{E} & -\boldsymbol{E} & \boldsymbol{O} \\ [\boldsymbol{r}_{1,\overline{\mathrm{cg-P}}}\times] & -[\boldsymbol{r}_{1,\overline{\mathrm{cg-D}}}\times] & \boldsymbol{O} \\ \boldsymbol{O} & \boldsymbol{E} & -\boldsymbol{E} \\ \boldsymbol{O} & [\boldsymbol{r}_{2,\overline{\mathrm{cg-P}}}\times] & -[\boldsymbol{r}_{2,\overline{\mathrm{cg-D}}}\times] \\ \boldsymbol{O} & \boldsymbol{O} & \boldsymbol{E} \\ \boldsymbol{O} & \boldsymbol{O} & [\boldsymbol{r}_{3,\overline{\mathrm{cg-P}}}\times] \end{bmatrix}, \boldsymbol{Q}=\begin{bmatrix} \boldsymbol{O} & \boldsymbol{O} & \boldsymbol{O} \\ \boldsymbol{E} & -\boldsymbol{E} & \boldsymbol{O} \\ \boldsymbol{O} & \boldsymbol{O} & \boldsymbol{O} \\ \boldsymbol{O} & \boldsymbol{E} & -\boldsymbol{E} \\ \boldsymbol{O} & \boldsymbol{O} & \boldsymbol{O} \\ \boldsymbol{O} & \boldsymbol{O} & \boldsymbol{E} \end{bmatrix}, \boldsymbol{H}=\begin{bmatrix} \boldsymbol{O}_{3\times1} \\ -\boldsymbol{\omega}_1\times(\hat{\boldsymbol{I}}_1\boldsymbol{\omega}_1) \\ \boldsymbol{O}_{3\times1} \\ -\boldsymbol{\omega}_2\times(\hat{\boldsymbol{I}}_2\boldsymbol{\omega}_2) \\ \boldsymbol{O}_{3\times1} \\ -\boldsymbol{\omega}_3\times(\hat{\boldsymbol{I}}_3\boldsymbol{\omega}_3) \end{bmatrix}, \boldsymbol{G}=\begin{bmatrix} m_1\boldsymbol{g} \\ \boldsymbol{O}_{3\times1} \\ m_2\boldsymbol{g} \\ \boldsymbol{O}_{3\times1} \\ m_3\boldsymbol{g} \\ \boldsymbol{O}_{3\times1} \end{bmatrix} \quad \text{(A4)}$$

** Figure A1 near here **

Assuming that every segment is connected to its adjacent segment at a joint, the geometric constraint for linked segments for all joints can be represented in matrix form as:

$$\boldsymbol{C}\dot{\boldsymbol{V}}+\dot{\boldsymbol{C}}\boldsymbol{V}=\ddot{\boldsymbol{\eta}}+\boldsymbol{B}\ddot{\boldsymbol{x}}_{\mathrm{Hip}} \quad \text{(A5)}$$

where $\boldsymbol{C}$ is the coefficient matrix for vector $\boldsymbol{V}$, and $\dot{\boldsymbol{\eta}}$ is the vector consisting of the differences between the distal and proximal point velocity vectors at individual joints (Koike et al., 2017). The matrix $\boldsymbol{B}$ is the coefficient matrix of hip joint acceleration $\ddot{\boldsymbol{x}}_{\mathrm{Hip}}$.

$$\boldsymbol{C}=\begin{bmatrix} -\boldsymbol{E} & [\boldsymbol{r}_{1,\overline{\mathrm{cg-P}}}\times] & \boldsymbol{O} & \boldsymbol{O} & \boldsymbol{O} & \boldsymbol{O} \\ \boldsymbol{E} & -[\boldsymbol{r}_{1,\overline{\mathrm{cg-D}}}\times] & -\boldsymbol{E} & [\boldsymbol{r}_{2,\overline{\mathrm{cg-P}}}\times] & \boldsymbol{O} & \boldsymbol{O} \\ \boldsymbol{O} & \boldsymbol{O} & \boldsymbol{E} & -[\boldsymbol{r}_{2,\overline{\mathrm{cg-D}}}\times] & -\boldsymbol{E} & [\boldsymbol{r}_{3,\overline{\mathrm{cg-P}}}\times] \end{bmatrix}, \boldsymbol{\eta}=\begin{bmatrix} \ddot{\boldsymbol{r}}^{*}_{1,\overline{\mathrm{cg-P}}} \\ \ddot{\boldsymbol{r}}^{*}_{2,\overline{\mathrm{cg-P}}}-\ddot{\boldsymbol{r}}^{*}_{1,\overline{\mathrm{cg-D}}} \\ \ddot{\boldsymbol{r}}^{*}_{3,\overline{\mathrm{cg-P}}}-\ddot{\boldsymbol{r}}^{*}_{2,\overline{\mathrm{cg-D}}} \end{bmatrix}, \boldsymbol{B}=\begin{bmatrix} -\boldsymbol{E} \\ \boldsymbol{O} \\ \boldsymbol{O} \end{bmatrix} \quad \text{(A6)}$$

$$\dot{\boldsymbol{C}}=\begin{bmatrix} \boldsymbol{O} & \left[\left(2\dot{\boldsymbol{r}}^{*}_{1,\overline{\mathrm{cg-P}}}+\boldsymbol{\omega}_1\times\boldsymbol{r}_{1,\overline{\mathrm{cg-P}}}\right)\times\right] & \boldsymbol{O} & \boldsymbol{O} & \boldsymbol{O} & \boldsymbol{O} \\ \boldsymbol{O} & -\left[\left(2\dot{\boldsymbol{r}}^{*}_{1,\overline{\mathrm{cg-D}}}+\boldsymbol{\omega}_1\times\boldsymbol{r}_{1,\overline{\mathrm{cg-D}}}\right)\times\right] & \boldsymbol{O} & \left[\left(2\dot{\boldsymbol{r}}^{*}_{2,\overline{\mathrm{cg-P}}}+\boldsymbol{\omega}_2\times\boldsymbol{r}_{2,\overline{\mathrm{cg-P}}}\right)\times\right] & \boldsymbol{O} & \boldsymbol{O} \\ \boldsymbol{O} & \boldsymbol{O} & \boldsymbol{O} & -\left[\left(2\dot{\boldsymbol{r}}^{*}_{2,\overline{\mathrm{cg-D}}}+\boldsymbol{\omega}_2\times\boldsymbol{r}_{2,\overline{\mathrm{cg-D}}}\right)\times\right] & \boldsymbol{O} & \left[\left(2\dot{\boldsymbol{r}}^{*}_{3,\overline{\mathrm{cg-P}}}+\boldsymbol{\omega}_3\times\boldsymbol{r}_{3,\overline{\mathrm{cg-P}}}\right)\times\right] \end{bmatrix} \quad \text{(A7)}$$

The equations for the anatomical constraint axes (e.g. varus/valgus axis at the knee joint), about which the joints cannot rotate freely, can be characterised as follows (Koike et al., 2017):

$$\boldsymbol{A}\dot{\boldsymbol{V}} + \dot{\boldsymbol{A}}\boldsymbol{V} = \ddot{\boldsymbol{\varphi}} \tag{A8}$$

where $\boldsymbol{A}$ is the coefficient matrix for the vector $\boldsymbol{V}$, and $\ddot{\boldsymbol{\varphi}}$ is the vector consisting of double differentiated values of the two-set of inner products (i.e. $\boldsymbol{e}_{1,x}^{\mathrm{T}}\boldsymbol{e}_{2,z} = \varphi_2$ at knee joint; $\boldsymbol{e}_{2,x}^{\mathrm{T}}\boldsymbol{e}_{3,z} = \varphi_3$ at ankle joint) of unit vectors of adjacent segments, expressing anatomical constraints.

Details of the matrices identified in the anatomical constraint equations in Equation A8 are as follows:

$$\boldsymbol{\varphi} = \begin{bmatrix}\varphi_2(t)\\ \varphi_3(t)\end{bmatrix}, \boldsymbol{A} = \begin{bmatrix}\boldsymbol{O}_{1\times3} & -\boldsymbol{e}_{2,z}^{\mathrm{T}}[\boldsymbol{e}_{1,x}\times] & \boldsymbol{O}_{1\times3} & -\boldsymbol{e}_{1,x}^{\mathrm{T}}[\boldsymbol{e}_{2,z}\times] & \boldsymbol{O}_{1\times3} & \boldsymbol{O}_{1\times3}\\ \boldsymbol{O}_{1\times3} & \boldsymbol{O}_{1\times3} & \boldsymbol{O}_{1\times3} & -\boldsymbol{e}_{3,z}^{\mathrm{T}}[\boldsymbol{e}_{2,x}\times] & \boldsymbol{O}_{1\times3} & -\boldsymbol{e}_{2,x}^{\mathrm{T}}[\boldsymbol{e}_{3,z}\times]\end{bmatrix} \tag{A9}$$

$$\dot{\boldsymbol{A}} = \begin{bmatrix}\boldsymbol{O}_{1\times3} & \dot{\boldsymbol{A}}_{1,2} & \boldsymbol{O}_{1\times3} & \dot{\boldsymbol{A}}_{1,4} & \boldsymbol{O}_{1\times3} & \boldsymbol{O}_{1\times3}\\ \boldsymbol{O}_{1\times3} & \boldsymbol{O}_{1\times3} & \boldsymbol{O}_{1\times3} & \dot{\boldsymbol{A}}_{2,4} & \boldsymbol{O}_{1\times3} & \dot{\boldsymbol{A}}_{2,6}\end{bmatrix}$$

$$\begin{cases}\dot{\boldsymbol{A}}_{1,2} = -(\boldsymbol{\omega}_2\times\boldsymbol{e}_{2,z})^{\mathrm{T}}[\boldsymbol{e}_{1,x}\times] - \boldsymbol{e}_{2,z}^{\mathrm{T}}[(\boldsymbol{\omega}_1\times\boldsymbol{e}_{1,x})\times],\\ \dot{\boldsymbol{A}}_{1,4} = -(\boldsymbol{\omega}_1\times\boldsymbol{e}_{1,x})^{\mathrm{T}}[\boldsymbol{e}_{2,z}\times] - \boldsymbol{e}_{1,x}^{\mathrm{T}}[(\boldsymbol{\omega}_2\times\boldsymbol{e}_{2,z})\times],\\ \dot{\boldsymbol{A}}_{2,4} = -(\boldsymbol{\omega}_3\times\boldsymbol{e}_{3,z})^{\mathrm{T}}[\boldsymbol{e}_{2,x}\times] - \boldsymbol{e}_{3,z}^{\mathrm{T}}[(\boldsymbol{\omega}_2\times\boldsymbol{e}_{2,x})\times],\\ \dot{\boldsymbol{A}}_{2,6} = -(\boldsymbol{\omega}_2\times\boldsymbol{e}_{2,x})^{\mathrm{T}}[\boldsymbol{e}_{3,z}\times] - \boldsymbol{e}_{2,x}^{\mathrm{T}}[(\boldsymbol{\omega}_3\times\boldsymbol{e}_{3,z})\times]\end{cases} \tag{A10}$$

The joint moment vector $\boldsymbol{N}$ is considered to be the sum of an active joint torque vector $\boldsymbol{T}_{\mathrm{a}}$ and a constraint joint torque vector $\boldsymbol{T}_{\mathrm{p}}$:

$$\boldsymbol{N} = \boldsymbol{S}_{\mathrm{a}}\boldsymbol{T}_{\mathrm{a}} + \boldsymbol{S}_{\mathrm{p}}\boldsymbol{T}_{\mathrm{p}} \tag{A11}$$

where the matrices $\boldsymbol{S}_{\mathrm{a}}$ and $\boldsymbol{S}_{\mathrm{p}}$ are the coefficient matrices for $\boldsymbol{T}_{\mathrm{a}}$ and $\boldsymbol{T}_{\mathrm{p}}$, respectively.

$$\boldsymbol{S}_a = \begin{bmatrix}\boldsymbol{K}_1^{-1} & \boldsymbol{O}_{3\times2} & \boldsymbol{O}_{3\times2}\\ \boldsymbol{O}_{3\times3} & \boldsymbol{K}_2^{-1}\begin{bmatrix}1&0&0\\0&0&1\end{bmatrix}^{\mathrm{T}} & \boldsymbol{O}_{3\times2}\\ \boldsymbol{O}_{3\times3} & \boldsymbol{O}_{3\times2} & \boldsymbol{K}_3^{-1}\begin{bmatrix}1&0&0\\0&0&1\end{bmatrix}^{\mathrm{T}}\end{bmatrix}, \boldsymbol{S}_p = \begin{bmatrix}\boldsymbol{O}_{3\times1} & \boldsymbol{O}_{3\times1}\\ \boldsymbol{K}_2^{-1}[0\quad 1\quad 0]^{\mathrm{T}} & \boldsymbol{O}_{3\times2}\\ \boldsymbol{O}_{3\times1} & \boldsymbol{K}_3^{-1}[0\quad 1\quad 0]^{\mathrm{T}}\end{bmatrix} \tag{A12}$$

$$\left.\begin{array}{c} \boldsymbol{K}_1 = [\boldsymbol{e}_{0,x} \quad \boldsymbol{e}'_{1,y} \quad \boldsymbol{e}_{1,z}],\ \boldsymbol{e}'_{1,y} = (\boldsymbol{e}_{1,z} \times \boldsymbol{e}_{0,x})/\|\boldsymbol{e}_{1,z} \times \boldsymbol{e}_{0,x}\| \\ \boldsymbol{K}_j = [\boldsymbol{e}_{j-1,x} \quad \boldsymbol{e}_{j,y} \quad \boldsymbol{e}_{j,z}], (j = 2,3) \end{array}\right\} \tag{A13}$$

where the unit vector $\boldsymbol{e}_{j,i}$ denotes the *i*-th axial vector of the *j*-th joint.

$$\boldsymbol{T}_a = [\tau_{1,x} \quad \tau_{1,y} \quad \tau_{1,z} \quad \tau_{2,x} \quad \tau_{2,z} \quad \tau_{3,x} \quad \tau_{3,z}]^{\mathrm{T}},\ \boldsymbol{T}_p = [\tau_{2,y} \quad \tau_{3,y}]^{\mathrm{T}} \tag{A14}$$

The gyroscopic effect moment vector $\boldsymbol{H}$ in Equation A1, which is also a function of the generalised velocity vector, can be expressed in the form of the product of the coefficient matrix $\bar{\boldsymbol{H}}$ and the generalised velocity vector $\boldsymbol{V}$ such that:

$$\boldsymbol{H}(\boldsymbol{V}) = \bar{\boldsymbol{H}}(\boldsymbol{V})\boldsymbol{V} \tag{A15}$$

Detail of the matrices identified in Equation A15 is as follows:

$$\bar{\boldsymbol{H}}(\boldsymbol{V}) = \text{block diag}\{\boldsymbol{O}, [(\hat{\boldsymbol{I}}_1\boldsymbol{\omega}_1)\times], \boldsymbol{O}, [(\hat{\boldsymbol{I}}_2\boldsymbol{\omega}_2)\times], \boldsymbol{O}, [(\hat{\boldsymbol{I}}_3\boldsymbol{\omega}_3)\times]\} \tag{A16}$$

Substituting Equations A5, A8 and A11 into Equation A1 yields a dynamic equation for the system as follows:

$$\begin{bmatrix} \dot{\boldsymbol{V}} \\ \boldsymbol{F} \\ \boldsymbol{T}_{\mathrm{p}} \end{bmatrix} = \begin{bmatrix} \boldsymbol{M} & -\boldsymbol{P} & -\boldsymbol{Q}\boldsymbol{S}_p \\ \boldsymbol{C} & \boldsymbol{O}_{9\times9} & \boldsymbol{O}_{9\times2} \\ \boldsymbol{A} & \boldsymbol{O}_{2\times9} & \boldsymbol{O}_{2\times2} \end{bmatrix}^{-1} \left\{ \begin{bmatrix} \boldsymbol{Q}\boldsymbol{S}_p \\ \boldsymbol{O}_{9\times7} \\ \boldsymbol{O}_{2\times7} \end{bmatrix} \boldsymbol{T}_{\mathrm{a}} + \begin{bmatrix} \bar{\boldsymbol{H}} \\ -\dot{\boldsymbol{C}} \\ -\dot{\boldsymbol{A}} \end{bmatrix} \boldsymbol{V} + \begin{bmatrix} \boldsymbol{E}_{18} \\ \boldsymbol{O}_{9\times18} \\ \boldsymbol{O}_{2\times18} \end{bmatrix} \boldsymbol{G} + \begin{bmatrix} \boldsymbol{O}_{18\times3} \\ \boldsymbol{B} \\ \boldsymbol{O}_{2\times3} \end{bmatrix} \ddot{\boldsymbol{x}}_{\mathrm{Hip}} + \begin{bmatrix} \boldsymbol{O}_{18\times9} \\ \boldsymbol{E}_9 \\ \boldsymbol{O}_{2\times9} \end{bmatrix} \ddot{\boldsymbol{\eta}} + \begin{bmatrix} \boldsymbol{O}_{18\times2} \\ \boldsymbol{O}_{9\times2} \\ \boldsymbol{E}_2 \end{bmatrix} \ddot{\boldsymbol{\varphi}} \right\} \tag{A17}$$

where the matrices $\boldsymbol{E}_n$ and $\boldsymbol{O}_{mxn}$ denote a unit matrix with *n* rows and columns, and the zero matrix with *m* rows and *n* columns, respectively.

Details of the matrices identified in the dynamical equations in Equations 2 and 3 are as follows.

$$\left.\begin{aligned}
&\boldsymbol{A_{V,Ta}} = \boldsymbol{M^{-1}WQ}_a,\\
&\bar{\boldsymbol{A}}_{\boldsymbol{V},\mathrm{MDT}} = \boldsymbol{M^{-1}W\bar{H}} + \boldsymbol{M^{-1}}\left\{\boldsymbol{P\bar{H}_{FV}} - \boldsymbol{Q}_p\left(\boldsymbol{\Gamma Q}_p\right)^{-1}\boldsymbol{\bar{H}_{TV}}\right\},\\
&\boldsymbol{A_{V,G}} = \boldsymbol{M^{-1}W},\\
&\boldsymbol{A}_{\boldsymbol{V},\mathrm{Hip}} = \boldsymbol{M^{-1}}\left\{\boldsymbol{P\bar{H}_{F\eta}} - \boldsymbol{Q}_p\left(\boldsymbol{\Gamma Q}_p\right)^{-1}\boldsymbol{\bar{H}_{T\eta}}\right\}\boldsymbol{B},\\
&\boldsymbol{A_{V,\eta}} = \boldsymbol{M^{-1}}\left\{\boldsymbol{P\bar{H}_{F\eta}} - \boldsymbol{Q}_p\left(\boldsymbol{\Gamma Q}_p\right)^{-1}\boldsymbol{\bar{H}_{T\eta}}\right\},\\
&\boldsymbol{A_{V,\varphi}} = \boldsymbol{M^{-1}}\left\{\boldsymbol{P\bar{H}_{F\varphi}} - \boldsymbol{Q}_p\left(\boldsymbol{\Gamma Q}_p\right)^{-1}\right\}
\end{aligned}\right\} \quad \text{(A18)}$$

where the temporary matrices $\boldsymbol{W}$, $\boldsymbol{\Phi}$, $\boldsymbol{Q}_a$, $\boldsymbol{Q}_b$, $\boldsymbol{\bar{H}_{FV}}$, $\boldsymbol{\Gamma}$, $\boldsymbol{\bar{H}_{TV}}$, $\boldsymbol{\bar{H}_{F\eta}}$, $\boldsymbol{\bar{H}_{T\eta}}$, $\boldsymbol{\bar{H}_{F\varphi}}$ and $\boldsymbol{B}$ are shown as follows:

$$\left.\begin{aligned}
&\boldsymbol{W} = \boldsymbol{P\Phi} - \boldsymbol{Q}_p\left(\boldsymbol{\Gamma Q}_p\right)^{-1}\boldsymbol{\Gamma} + \boldsymbol{E},\\
&\boldsymbol{\Phi} = \left(\boldsymbol{CM^{-1}P}\right)^{-1}\boldsymbol{CM^{-1}}\left\{\boldsymbol{Q}_p\left(\boldsymbol{\Gamma Q}_p\right)^{-1}\boldsymbol{\Gamma} - \boldsymbol{E}\right\},\\
&\boldsymbol{Q}_a = \boldsymbol{QS}_a,\\
&\boldsymbol{Q}_p = \boldsymbol{QS}_p,\\
&\boldsymbol{\bar{H}_{FV}} = \left(\boldsymbol{CM^{-1}P}\right)^{-1}\{\boldsymbol{CM^{-1}Q}_p\left(\boldsymbol{\Gamma Q}_p\right)^{-1}\boldsymbol{\bar{H}_{TV}} - \dot{\boldsymbol{C}}\},\\
&\boldsymbol{\Gamma} = \boldsymbol{AM^{-1}}\{\boldsymbol{E} - \boldsymbol{P}\left(\boldsymbol{CM^{-1}P}\right)^{-1}\boldsymbol{CM^{-1}}\},\\
&\boldsymbol{\bar{H}_{TV}} = \dot{\boldsymbol{A}} - \boldsymbol{AM^{-1}P}\left(\boldsymbol{CM^{-1}P}\right)^{-1}\dot{\boldsymbol{C}},\\
&\boldsymbol{\bar{H}_{F\eta}} = \left(\boldsymbol{CM^{-1}P}\right)^{-1}\left\{\boldsymbol{CM^{-1}Q}_p\left(\boldsymbol{\Gamma Q}_p\right)^{-1}\boldsymbol{\bar{H}_{T\eta}} + \boldsymbol{E}\right\},\\
&\boldsymbol{\bar{H}_{T\eta}} = \boldsymbol{AM^{-1}P}\left(\boldsymbol{CM^{-1}P}\right)^{-1},\\
&\boldsymbol{\bar{H}_{F\varphi}} = \left(\boldsymbol{CM^{-1}P}\right)^{-1}\boldsymbol{CM^{-1}Q}_p\left(\boldsymbol{\Gamma Q}_p\right)^{-1},\\
&\boldsymbol{B} = [\boldsymbol{E}_3 \quad \boldsymbol{O}_{3\times3} \quad \boldsymbol{O}_{3\times3}]^T
\end{aligned}\right\} \quad \text{(A19)}$$

Appendix 2

The contribution of each term at every instant to the generation of the generalised velocity vector can be derived from Figure 2b which represents Equation 9. For example, the generalised velocity vector at time *k* can be calculated from the time history of the input vector $\dot{\boldsymbol{V}}_{\mathrm{Dir}}(k)$ as follows:

$$\boldsymbol{V}(k) = \Delta t\dot{\boldsymbol{V}}_{\mathrm{Dir}}(k-1) + \Delta t\sum_{h=1}^{k-1}\left[\left\{\prod_{j=h}^{k-1}\widetilde{\boldsymbol{\Psi}}_{\boldsymbol{V}}(j)\right\}\dot{\boldsymbol{V}}_{\mathrm{Dir}}(h-1)\right] + \left\{\prod_{j=0}^{k-1}\widetilde{\boldsymbol{\Psi}}_{\boldsymbol{V}}(j)\right\}\boldsymbol{V}(0) \quad \text{(A20)}$$

where the function $\boldsymbol{\Pi}$ denotes the factorial function shown as

$$\prod_{j=h}^{k}\widetilde{\boldsymbol{\Psi}}_{\boldsymbol{V}}(j) = \widetilde{\boldsymbol{\Psi}}_{\boldsymbol{V}}(k)\widetilde{\boldsymbol{\Psi}}_{\boldsymbol{V}}(k-1)\widetilde{\boldsymbol{\Psi}}_{\boldsymbol{V}}(k-2)\cdots\widetilde{\boldsymbol{\Psi}}_{\boldsymbol{V}}(h) \quad \text{(A21)}$$

The generalised velocity vector at time k can be obtained from Equations A20 and A21 as the sums of individual contributions as follows:

$$\boldsymbol{V}(k) = \boldsymbol{C}_{\boldsymbol{V},\boldsymbol{T}\mathrm{a}}(k) + \boldsymbol{C}_{\boldsymbol{V},\boldsymbol{G}}(k) + \boldsymbol{C}_{\boldsymbol{V},\boldsymbol{V_0}}(k) + \boldsymbol{C}_{\boldsymbol{V},\mathrm{other}}(k),$$

$$\begin{cases} \boldsymbol{C}_{\boldsymbol{V},\boldsymbol{T}\mathrm{a}}(k) = \Delta t \boldsymbol{A}_{\boldsymbol{V},\boldsymbol{T}a}(k-1)\boldsymbol{T}_a(k-1) + \Delta t \sum_{h=1}^{k-1}\left[\left\{\prod_{j=h}^{k-1}\widetilde{\boldsymbol{\Psi}}_{\boldsymbol{V}}(j)\right\}\boldsymbol{A}_{\boldsymbol{V},\boldsymbol{T}a}(h-1)\boldsymbol{T}_a(h-1)\right], \\ \boldsymbol{C}_{\boldsymbol{V},\boldsymbol{G}}(k) = \Delta t \boldsymbol{A}_{\boldsymbol{V},\boldsymbol{G}}(k-1)\boldsymbol{G} + \Delta t \sum_{h=0}^{k-1}\left[\left\{\prod_{j=h}^{k-1}\widetilde{\boldsymbol{\Psi}}_{\boldsymbol{V}}(j)\right\}\boldsymbol{A}_{\boldsymbol{V},\boldsymbol{G}}(h-1)\boldsymbol{G}\right], \\ \boldsymbol{C}_{\boldsymbol{V},\boldsymbol{V_0}}(k) = \left\{\prod_{j=0}^{k-1}\widetilde{\boldsymbol{\Psi}}_{\boldsymbol{V}}(j)\right\}\boldsymbol{V}(0) \end{cases} \quad \text{(A22)}$$

where the vectors $\boldsymbol{C}_{\boldsymbol{V},Ta}$, $\boldsymbol{C}_{\boldsymbol{V},\boldsymbol{G}}$, $\boldsymbol{C}_{\boldsymbol{V},\boldsymbol{V_0}}$ and $\boldsymbol{C}_{\boldsymbol{V},\mathrm{other}}$ respectively denote total contributions of the active joint torque, gravity, the initial velocity term, and other terms (as expressed in Equation A23) to the generation of the generalised velocity vector $\boldsymbol{V}(k)$ in consideration of the generating factors of the MDT.

The vectors $\boldsymbol{C}_{\boldsymbol{V},\mathrm{Hip}}$, $\boldsymbol{C}_{\boldsymbol{V},\eta}$ and $\boldsymbol{C}_{\boldsymbol{V},\varphi}$ denote total contributions of the hip-joint acceleration term, segment length fluctuation term, and constraint joint axial angle fluctuation term, respectively.

$$\boldsymbol{C}_{\boldsymbol{V},\mathrm{other}}(k) = \boldsymbol{C}_{\boldsymbol{V},\mathrm{Hip}}(k) + \boldsymbol{C}_{\boldsymbol{V},\boldsymbol{\eta}}(k) + \boldsymbol{C}_{\boldsymbol{V},\boldsymbol{\varphi}}(k),$$

$$\begin{cases} \boldsymbol{C}_{\boldsymbol{V},\mathrm{Hip}}(k) = \Delta t \boldsymbol{A}_{\boldsymbol{V},\mathrm{Hip}}(k-1)\ddot{\boldsymbol{x}}_{\mathrm{Hip}}(k-1) + \Delta t \sum_{h=1}^{k-1}\left[\left\{\prod_{j=h}^{k-1}\widetilde{\boldsymbol{\Psi}}_{\boldsymbol{V}}(j)\right\}\boldsymbol{A}_{\boldsymbol{V},\mathrm{Hip}}(h-1)\ddot{\boldsymbol{x}}_{\mathrm{Hip}}(h-1)\right], \\ \boldsymbol{C}_{\boldsymbol{V},\boldsymbol{\eta}}(k) = \Delta t \boldsymbol{A}_{\boldsymbol{V},\boldsymbol{\eta}}(k-1)\ddot{\boldsymbol{\eta}}(k-1) + \Delta t \sum_{h=1}^{k-1}\left[\left\{\prod_{j=h}^{k-1}\widetilde{\boldsymbol{\Psi}}_{\boldsymbol{V}}(j)\right\}\boldsymbol{A}_{\boldsymbol{V},\boldsymbol{\eta}}(h-1)\ddot{\boldsymbol{\eta}}(h-1)\right], \\ \boldsymbol{C}_{\boldsymbol{V},\boldsymbol{\varphi}}(k) = \Delta t \boldsymbol{A}_{\boldsymbol{V},\boldsymbol{\varphi}}(k-1)\ddot{\boldsymbol{\varphi}}(k-1) + \Delta t \sum_{h=1}^{k-1}\left[\left\{\prod_{j=h}^{k-1}\widetilde{\boldsymbol{\Psi}}_{\boldsymbol{V}}(j)\right\}\boldsymbol{A}_{\boldsymbol{V},\boldsymbol{\varphi}}(h-1)\ddot{\boldsymbol{\varphi}}(h-1)\right] \end{cases} \quad \text{(A23)}$$

The generalised velocity vector at time k can be obtained from Equations 4, 5 and 7 as the sums of individual contributions as follows:

$$\boldsymbol{V}(k) = \boldsymbol{C}_{\mathrm{Dir},\boldsymbol{V},\boldsymbol{T}\mathrm{a}}(k) + \boldsymbol{C}_{\mathrm{Dir},\boldsymbol{V},\mathrm{MDT}}(k) + \boldsymbol{C}_{\mathrm{Dir},\boldsymbol{V},\boldsymbol{G}}(k) + \boldsymbol{C}_{\mathrm{Dir},\boldsymbol{V},\mathrm{other}}(k) + \boldsymbol{V}(0),$$

$$\begin{cases} \boldsymbol{C}_{\mathrm{Dir},\boldsymbol{V},\boldsymbol{T}\mathrm{a}}(k) = \Delta t \sum_{h=0}^{k-1} \boldsymbol{A}_{\boldsymbol{V},\boldsymbol{T}\mathrm{a}}(h)\boldsymbol{T}_{\mathrm{a}}(h), & \boldsymbol{C}_{\mathrm{Dir},\boldsymbol{V},\mathrm{MDT}}(k) = \Delta t \sum_{h=0}^{k-1} \bar{\boldsymbol{A}}_{\boldsymbol{V},\mathrm{MDT}}(\boldsymbol{V}(h))\boldsymbol{V}(h), \\ \boldsymbol{C}_{\mathrm{Dir},\boldsymbol{V},\boldsymbol{G}}(k) = \Delta t \sum_{h=0}^{k-1} \boldsymbol{A}_{\boldsymbol{V},\boldsymbol{G}}(h)\boldsymbol{G}, & \boldsymbol{C}_{\mathrm{Dir},\boldsymbol{V},\mathrm{other}}(k) = \Delta t \sum_{h=0}^{k-1} \boldsymbol{A}_{\boldsymbol{V},\mathrm{other}}(h) \end{cases} \tag{A24}$$

where the contribution vectors $\boldsymbol{C}_{\mathrm{Dir},\boldsymbol{V},\boldsymbol{T}a}$, $\boldsymbol{C}_{\mathrm{Dir},\boldsymbol{V},\mathrm{MDT}}$, $\boldsymbol{C}_{\mathrm{Dir},\boldsymbol{V},\mathbf{G}}$ and $\boldsymbol{C}_{\mathrm{Dir},\boldsymbol{V},\mathrm{other}}$ respectively denote direct effects of the active joint torque, the motion-dependent term, the gravitational term, and other terms to the generation of the generalised velocity vector $\boldsymbol{V}(k)$.

Furthermore, the direct effect of active joint torque input can be distributed into the sums of the direct effects of the individual joint torque inputs as:

$$\begin{aligned} \boldsymbol{C}_{\mathrm{Dir},\boldsymbol{V},\boldsymbol{T}\mathrm{a}}(k) &= \sum_{j_{\mathrm{Axis}}=1}^{n_{\mathrm{Axis}}} \boldsymbol{C}_{\mathrm{Dir},\boldsymbol{V},\boldsymbol{T}\mathrm{a},j_{\mathrm{Axis}}}(k), \\ \boldsymbol{C}_{\mathrm{Dir},\boldsymbol{V},\boldsymbol{T}\mathrm{a},j_{\mathrm{Axis}}}(k) &= \Delta t \sum_{h=0}^{k-1} \boldsymbol{A}_{\boldsymbol{V},\boldsymbol{T}\mathrm{a},j_{\mathrm{Axis}}}(h)\boldsymbol{T}_{\mathrm{a},j_{\mathrm{Axis}}}(h) \end{aligned} \tag{A25}$$

where n_{Axis} denotes the number of the active joint axes.

The total contribution is the sum of the direct and indirect effects of joint torque inputs:

$$\boldsymbol{C}_{\boldsymbol{V},\boldsymbol{T}\mathrm{a}}(k) = \boldsymbol{C}_{\mathrm{Dir},\boldsymbol{V},\boldsymbol{T}\mathrm{a}}(k) + \boldsymbol{C}_{\mathrm{Indir},\boldsymbol{V},\boldsymbol{T}\mathrm{a}}(k) \tag{A26}$$

The indirect effect of the joint torque inputs is obtained from the difference between the total contribution and the direct effect of joint torque inputs from Equation A26 as:

$$\boldsymbol{C}_{\mathrm{Indir},\boldsymbol{V},\boldsymbol{T}\mathrm{a}}(k) = \boldsymbol{C}_{\boldsymbol{V},\boldsymbol{T}\mathrm{a}}(k) - \boldsymbol{C}_{\mathrm{Dir},\boldsymbol{V},\boldsymbol{T}\mathrm{a}}(k) \tag{A27}$$

Contributions to the kicking foot CG's speed

As described in Equation A2, the linear velocity vector of the CG of the kicking foot $\dot{\boldsymbol{x}}_3(k)$ can be expressed as follows:

$$\dot{\boldsymbol{x}}_3(k) = \boldsymbol{S}_3\boldsymbol{V}(k), \qquad \boldsymbol{S}_3 = [\boldsymbol{O}_{3\times12} \quad \boldsymbol{E} \quad \boldsymbol{O}_{3\times3}] \tag{A28}$$

where the matrix $\boldsymbol{S}_3(k)$ indicates the selective matrix which extracts the components of the linear velocity vector regarding the foot segment from the generalised velocity vector.

The unit vector, expressing the direction of the foot CG's velocity vector, is obtained by dividing the velocity vector by its magnitude as:

$$\boldsymbol{e}_3(k) = \frac{\dot{\boldsymbol{x}}_3(k)}{|\dot{\boldsymbol{x}}_3(k)|} \tag{A29}$$

Finally, operating the inner product of Equation A29 with Equations A24 through A28 yields the dynamic contributions of individual terms to the generation of the point's speed at time k, $s_3(k)$, shown as:

$$s_3(k) = C_{s3,Ta}(k) + C_{s3,G}(k) + C_{s3,\text{other}}(k) + C_{s3,V_0}(k) \tag{A30}$$

where the terms $C_{s3,\text{Ta}}(k)$, $C_{s3,\text{G}}(k)$ and $C_{s3,\text{other}}(k)$ respectively denote the contributions of the joint torque term, gravitational term and other terms to the foot CG's speed. The term $C_{\text{s3},V_0}(k)$ denotes the contribution of the initial velocity term, i.e. the velocity of the system at the start of the analysis.

For example, the contribution of the active joint torque to the generation of the foot CG's speed at time k is expressed as follows:

$$C_{s3,\boldsymbol{T}\mathrm{a}}(k) = \boldsymbol{e}_3^{\mathrm{T}}(k)\overline{\boldsymbol{S}}_3\left(\Delta t\boldsymbol{A}_{\boldsymbol{V},\boldsymbol{T}a}(k-1)\boldsymbol{T}_a(k-1) + \Delta t\sum_{h=1}^{k-1}\left[\left\{\prod_{j=h}^{k-1}\widetilde{\boldsymbol{\Psi}}_{\boldsymbol{V}}(j)\right\}\boldsymbol{A}_{\boldsymbol{V},\boldsymbol{T}a}(h-1)\boldsymbol{T}_a(h-1)\right]\right) \quad \text{(A31)}$$

$$C_{\mathrm{Dir},s3,\boldsymbol{T}\mathrm{a}}(k) = \boldsymbol{e}_3^{\mathrm{T}}(k)\overline{\boldsymbol{S}}_3\Delta t\sum_{h=0}^{k-1}\boldsymbol{A}_{\boldsymbol{V},\boldsymbol{T}\mathrm{a}}(h)\boldsymbol{T}_{\mathrm{a}}(h), \quad \text{(A32)}$$

$$\begin{aligned} C_{\mathrm{Indir},s3,\boldsymbol{T}\mathrm{a}}(k) &= C_{\mathrm{s3},\boldsymbol{T}\mathrm{a}}(k) - C_{\mathrm{Dir},s3,\boldsymbol{T}\mathrm{a}}(k) \\ &= \boldsymbol{e}_3^{\mathrm{T}}(k)\overline{\boldsymbol{S}}_3\Delta t\sum_{h=1}^{k-1}\left(\left\{\prod_{j=h}^{k-1}\widetilde{\boldsymbol{\Psi}}_{\boldsymbol{V}}(j)\right\} - \boldsymbol{E}_{18}\right)\boldsymbol{A}_{\boldsymbol{V},\boldsymbol{T}\mathrm{a}}(h-1)\boldsymbol{T}_{\mathrm{a}}(h-1) \end{aligned} \quad \text{(A33)}$$

According to Equations A31 and A32, the direct and indirect effects of a joint torque inputted at time h (any given instant in time between swing start and time k), $C_{\mathrm{Inst},s3,\mathrm{BC},\boldsymbol{T}a}(h)$ and $C_{\mathrm{Cumul},s3,\mathrm{BC},\boldsymbol{T}a}(h)$ to the generation of the foot CG's speed at BC are expressed as follows:

$$C_{\mathrm{Dir},s3,\mathrm{BC},\boldsymbol{T}\mathrm{a}}(h) = \boldsymbol{e}_3^{\mathrm{T}}(k_{\mathrm{BC}})\overline{\boldsymbol{S}}_3\Delta t\boldsymbol{A}_{\boldsymbol{V},\boldsymbol{T}\mathrm{a}}(h)\boldsymbol{T}_{\mathrm{a}}(h), \quad \text{(A34)}$$

$$C_{\mathrm{Indir},s3,\mathrm{BC},\boldsymbol{T}\mathrm{a}}(h) = \boldsymbol{e}_3^{\mathrm{T}}(k_{\mathrm{BC}})\overline{\boldsymbol{S}}_3\Delta t\left(\left\{\prod_{j=h+1}^{k_{\mathrm{BC}}-1}\widetilde{\boldsymbol{\Psi}}_{\boldsymbol{V}}(j)\right\} - \boldsymbol{E}_{18}\right)\boldsymbol{A}_{\boldsymbol{V},\boldsymbol{T}\mathrm{a}}(h)\boldsymbol{T}_{\mathrm{a}}(h) \quad \text{(A35)}$$

The individual contributions of the active joint torques, expressed by Equations A31 through A35, can be furthermore divided into the contributions of the individual active joint torques about each individual axis of a joint (not shown).

Appendix 3

Decomposition of the MDT into kinematic components

The contribution of the MDT to the generalised acceleration vector can be expressed in the following form when using

Equation A17:

$$\boldsymbol{C}_{\dot{\boldsymbol{V}},\mathrm{MDT}} = \bar{\boldsymbol{A}}_{\boldsymbol{V},\mathrm{MDT}}(\boldsymbol{V})\boldsymbol{V} = \boldsymbol{S}_{\dot{\boldsymbol{V}}}\boldsymbol{B}_{\mathrm{sys}}\begin{bmatrix}\bar{\boldsymbol{H}}\\ -\dot{\boldsymbol{C}}\\ -\dot{\boldsymbol{A}}\end{bmatrix}\boldsymbol{V},$$

$$\boldsymbol{S}_{\dot{\boldsymbol{V}}} = [\boldsymbol{E}_{18} \quad \boldsymbol{O}_{18\times 9} \quad \boldsymbol{O}_{18\times 2}], \qquad \boldsymbol{B}_{\mathrm{sys}} = \begin{bmatrix}\boldsymbol{M} & -\boldsymbol{P} & -\boldsymbol{Q}\boldsymbol{S}_p\\ \boldsymbol{C} & \boldsymbol{O}_{9\times 9} & \boldsymbol{O}_{9\times 2}\\ \boldsymbol{A} & \boldsymbol{O}_{2\times 9} & \boldsymbol{O}_{2\times 2}\end{bmatrix}^{-1} \tag{A36}$$

where matrix $\boldsymbol{S}_{\dot{\boldsymbol{V}}}$ denotes the selective matrix extracting the generalised acceleration components from Equation A17, and matrix $\boldsymbol{B}_{\mathrm{sys}}$ indicates the coefficient matrix of the target system shown in Equation A17. This equation can be expressed as the sum of three terms, as shown in the following equation:

$$\boldsymbol{C}_{\dot{\boldsymbol{V}},\mathrm{MDT}} = \boldsymbol{S}_{\dot{\boldsymbol{V}}}\boldsymbol{B}_{\mathrm{sys}}\begin{bmatrix}\bar{\boldsymbol{H}}\boldsymbol{V}\\ \boldsymbol{O}_{9\times 1}\\ \boldsymbol{O}_{2\times 1}\end{bmatrix} - \boldsymbol{S}_{\dot{\boldsymbol{V}}}\boldsymbol{B}_{\mathrm{sys}}\begin{bmatrix}\boldsymbol{O}_{18\times 1}\\ \dot{\boldsymbol{C}}_{\boldsymbol{B}}\boldsymbol{V}\\ \boldsymbol{O}_{2\times 1}\end{bmatrix} - \boldsymbol{S}_{\dot{\boldsymbol{V}}}\boldsymbol{B}_{\mathrm{sys}}\begin{bmatrix}\boldsymbol{O}_{18\times 1}\\ \dot{\boldsymbol{C}}_{\boldsymbol{C}}\boldsymbol{V}\\ \dot{\boldsymbol{A}}\boldsymbol{V}\end{bmatrix},$$

$$\begin{cases}\dot{\boldsymbol{C}}_{\boldsymbol{B}} = \begin{bmatrix}\boldsymbol{O} & [2\dot{\boldsymbol{r}}^{*}_{1,\overline{\mathrm{cg-P}}}\times] & \boldsymbol{O} & \boldsymbol{O} & \boldsymbol{O} & \boldsymbol{O}\\ \boldsymbol{O} & -[2\dot{\boldsymbol{r}}^{*}_{1,\overline{\mathrm{cg-D}}}\times] & \boldsymbol{O} & [2\dot{\boldsymbol{r}}^{*}_{2,\overline{\mathrm{cg-P}}}\times] & \boldsymbol{O} & \boldsymbol{O}\\ \boldsymbol{O} & \boldsymbol{O} & \boldsymbol{O} & -[2\dot{\boldsymbol{r}}^{*}_{2,\overline{\mathrm{cg-D}}}\times] & \boldsymbol{O} & [2\dot{\boldsymbol{r}}^{*}_{3,\overline{\mathrm{cg-P}}}\times]\end{bmatrix},\\ \dot{\boldsymbol{C}}_{\boldsymbol{C}} = \begin{bmatrix}\boldsymbol{O} & [(\boldsymbol{\omega}_1\times\boldsymbol{r}_{1,\overline{\mathrm{cg-P}}})\times] & \boldsymbol{O} & \boldsymbol{O} & \boldsymbol{O} & \boldsymbol{O}\\ \boldsymbol{O} & -[(\boldsymbol{\omega}_1\times\boldsymbol{r}_{1,\overline{\mathrm{cg-D}}})\times] & \boldsymbol{O} & [(\boldsymbol{\omega}_2\times\boldsymbol{r}_{2,\overline{\mathrm{cg-P}}})\times] & \boldsymbol{O} & \boldsymbol{O}\\ \boldsymbol{O} & \boldsymbol{O} & \boldsymbol{O} & -[(\boldsymbol{\omega}_2\times\boldsymbol{r}_{2,\overline{\mathrm{cg-D}}})\times] & \boldsymbol{O} & [(\boldsymbol{\omega}_3\times\boldsymbol{r}_{3,\overline{\mathrm{cg-P}}})\times]\end{bmatrix}\end{cases} \tag{A37}$$

where the terms on the right side of this equation represent, in turn, the gyroscopic effect moment component, the segment length fluctuation component, and the centrifugal and Coriolis forces component of the contribution of the MDT to the generalised acceleration vector. Matrices $\dot{\boldsymbol{C}}_{\boldsymbol{B}}$ and $\dot{\boldsymbol{C}}_{\boldsymbol{C}}$ denote the coefficient matrices with respect to the generalised velocity vector and their sum is equal to $\dot{\boldsymbol{C}}$ in Equation A7.

The angular velocity vector of the *i*-th segment is expressed as the sum of $\boldsymbol{\omega}_0$ and the summation of the products of multiplying the joint angular velocity $\dot{\theta}_{i_c,l_c}$ by the unit vector of the joint axial vector $\boldsymbol{e}_{i_c,l_c}$ as:

$$\boldsymbol{\omega}_i = \boldsymbol{\omega}_0 + \sum_{i_c=1}^{i}\sum_{l_c=1}^{n(i_c)}\dot{\theta}_{i_c,l_c}\boldsymbol{e}_{i_c,l_c}, \ n=[3,2,2], \ i=1,2,3 \tag{A38}$$

$$\begin{cases} \boldsymbol{e}_{1,1} = \boldsymbol{e}_{0,x}, & \boldsymbol{e}_{1,2} = \boldsymbol{e}'_{1,y}, & \boldsymbol{e}_{1,3} = \boldsymbol{e}_{1,z}, \\ \boldsymbol{e}_{2,1} = \boldsymbol{e}_{1,x}, & \boldsymbol{e}_{2,2} = \boldsymbol{e}_{2,z}, & \\ \boldsymbol{e}_{3,1} = \boldsymbol{e}_{2,x}, & \boldsymbol{e}_{3,2} = \boldsymbol{e}_{3,z} & \end{cases}$$

where the vector $\boldsymbol{e}'_{1,y}$ is the unit vector defined in Equation A13, and i_c and l_c are dummy variables used in the summation.

The components of the vector $\dot{\boldsymbol{A}}\boldsymbol{V}$, which is in the third term of the right-side of Equation A37, are expressed by the following equation from Equation A10:

$$\dot{\boldsymbol{A}}\boldsymbol{V} = \begin{bmatrix} -2(\boldsymbol{\omega}_2 \times \boldsymbol{e}_{2,z})^{\mathrm{T}}(\boldsymbol{e}_{1,x} \times \boldsymbol{\omega}_1) - \boldsymbol{e}_{2,z}^{\mathrm{T}}[(\boldsymbol{\omega}_1 \times \boldsymbol{e}_{1,x}) \times \boldsymbol{\omega}_1] - \boldsymbol{e}_{1,x}^{\mathrm{T}}[(\boldsymbol{\omega}_2 \times \boldsymbol{e}_{2,z}) \times \boldsymbol{\omega}_2] \\ -2(\boldsymbol{\omega}_3 \times \boldsymbol{e}_{3,z})^{\mathrm{T}}(\boldsymbol{e}_{2,x} \times \boldsymbol{\omega}_2) - \boldsymbol{e}_{3,z}^{\mathrm{T}}[(\boldsymbol{\omega}_2 \times \boldsymbol{e}_{2,x}) \times \boldsymbol{\omega}_2] - \boldsymbol{e}_{2,x}^{\mathrm{T}}[(\boldsymbol{\omega}_3 \times \boldsymbol{e}_{3,z}) \times \boldsymbol{\omega}_3] \end{bmatrix} \tag{A39}$$

The components of the vector $\dot{\boldsymbol{C}}_{\boldsymbol{C}}\boldsymbol{V}$ are expressed by the following equation:

$$\dot{\boldsymbol{C}}_{\boldsymbol{C}}\boldsymbol{V} = \begin{bmatrix} (\boldsymbol{\omega}_1 \times \boldsymbol{r}_{1,\overline{\mathrm{cg-P}}}) \times \boldsymbol{\omega}_1 \\ -(\boldsymbol{\omega}_1 \times \boldsymbol{r}_{1,\overline{\mathrm{cg-D}}}) \times \boldsymbol{\omega}_1 + (\boldsymbol{\omega}_2 \times \boldsymbol{r}_{2,\overline{\mathrm{cg-P}}}) \times \boldsymbol{\omega}_2 \\ -(\boldsymbol{\omega}_2 \times \boldsymbol{r}_{2,\overline{\mathrm{cg-D}}}) \times \boldsymbol{\omega}_2 + (\boldsymbol{\omega}_3 \times \boldsymbol{r}_{3,\overline{\mathrm{cg-P}}}) \times \boldsymbol{\omega}_3 \end{bmatrix} \tag{A40}$$

When considering the angular velocity vector of the i-th segment as given in Equation A38, any element expressed as $(\boldsymbol{\omega}_i \times \boldsymbol{r}_{i,s}) \times \boldsymbol{\omega}_i$ can be divided into five components that arise from either centrifugal forces or Coriolis forces:

$$\begin{aligned} (\boldsymbol{\omega}_i \times \boldsymbol{r}_{i,s}) \times \boldsymbol{\omega}_i = \; & (\boldsymbol{\omega}_0 \times \boldsymbol{r}_{i,s}) \times \boldsymbol{\omega}_0 && \text{: Centrifugal force term} \\ & + \sum_{i_c=1}^{i} \sum_{l_c=1}^{n(i_c)} \dot{\theta}_{i_c,l_c}{}^2 (\boldsymbol{e}_{i_c,l_c} \times \boldsymbol{r}_{i,s}) \times \boldsymbol{e}_{i_c,l_c} && \text{: Centrifugal force term} \\ & + \left\{ \left(\sum_{i_c=1}^{i} \sum_{l_c=1}^{n(i_c)} \dot{\theta}_{i_c,l_c} \boldsymbol{e}_{i_c,l_c} \right) \times \boldsymbol{r}_{i,s} \right\} \times \boldsymbol{\omega}_0 && \text{: Coriolis force term} \\ & + (\boldsymbol{\omega}_0 \times \boldsymbol{r}_{i,s}) \times \left(\sum_{i_c=1}^{i} \sum_{l_c=1}^{n(i_c)} \dot{\theta}_{i_c,l_c} \boldsymbol{e}_{i_c,l_c} \right) && \text{: Coriolis force term} \\ & + \sum_{j_c=1}^{j} \sum_{h_c=1}^{n(j_c)} \sum_{i_c=1}^{i} \sum_{l_c=1}^{n(i_c)} \{ \alpha_{j_c,h_c,i_c,l_c} \dot{\theta}_{i_c,l_c} \dot{\theta}_{j_c,h_c} (\boldsymbol{e}_{i_c,l_c} \times \boldsymbol{r}_{i,s}) \times \boldsymbol{e}_{j_c,h_c} \}, && \text{: Coriolis force term} \\ & n = [3,2,2] \end{aligned} \tag{A41}$$

where j_c and h_c are additional dummy variables used in the summations, and the coefficient in the fifth term in the right side of Equation A41 α_{j_c,h_c,i_c,l_c} is given as:

$$\alpha_{j_c,h_c,i_c,l_c} = \begin{cases} 0: & \text{if } j_c = i_c \text{ and } h_c = l_c \\ 1: & \text{else} \end{cases} \tag{A42}$$

and the subscript s of the position vector $\boldsymbol{r}_{i,s}$ denotes $\overline{\text{cg}-\text{D}}$ or $\overline{\text{cg}-\text{P}}$.

Any element expressed as $\left(\boldsymbol{\omega}_i \times \boldsymbol{e}_{i,z}\right)^{\mathrm{T}}\left(\boldsymbol{e}_{j,x} \times \boldsymbol{\omega}_j\right)$ in Equation A39 can be divided into five components representing either centrifugal force terms or Coriolis force terms:

$$\begin{aligned} \left(\boldsymbol{\omega}_i \times \boldsymbol{e}_{i,z}\right)^{\mathrm{T}}\left(\boldsymbol{e}_{j,x} \times \boldsymbol{\omega}_j\right) = \quad & \left(\boldsymbol{\omega}_0 \times \boldsymbol{e}_{i,z}\right)^{\mathrm{T}}\left(\boldsymbol{e}_{j,x} \times \boldsymbol{\omega}_0\right) && \text{: Centrifugal force term} \\ & + \sum_{j_c=1}^{j} \sum_{h_c=1}^{n(j_c)} \dot{\theta}_{j_c,h_c}{}^2 \left(\boldsymbol{e}_{j_c,h_c} \times \boldsymbol{e}_{i,z}\right)^{\mathrm{T}}\left(\boldsymbol{e}_{j,x} \times \boldsymbol{e}_{j_c,h_c}\right) && \text{: Centrifugal force term} \\ & + \left(\boldsymbol{\omega}_0 \times \boldsymbol{e}_{i,z}\right)^{\mathrm{T}} \left\{ \boldsymbol{e}_{j,x} \times \left(\sum_{j_c=1}^{j} \sum_{h_c=1}^{n(j_c)} \dot{\theta}_{j_c,h_c} \boldsymbol{e}_{j_c,h_c} \right) \right\} && \text{: Coriolis force term} \\ & + \left(\boldsymbol{\omega}_0 \times \boldsymbol{e}_{j,x}\right)^{\mathrm{T}} \left\{ \boldsymbol{e}_{i,z} \times \left(\sum_{i_c=1}^{i} \sum_{l_c=1}^{n(i_c)} \dot{\theta}_{i_c,l_c} \boldsymbol{e}_{i_c,l_c} \right) \right\} && \text{: Coriolis force term} \\ & + \sum_{j_c=1}^{j} \sum_{h_c=1}^{n(j_c)} \sum_{i_c=1}^{i} \sum_{l_c=1}^{n(i_c)} \left\{ \alpha_{j_c,h_c,i_c,l_c} \dot{\theta}_{i_c,l_c} \dot{\theta}_{j_c,h_c} \left(\boldsymbol{e}_{i_c,l_c} \times \boldsymbol{e}_{i,z}\right)^{\mathrm{T}}\left(\boldsymbol{e}_{j,x} \times \boldsymbol{e}_{j_c,h_c}\right) \right\} \\ & && \text{: Coriolis force term } , (j < i),\ n = [3,2,2] \end{aligned} \tag{A43}$$

From Equations A40, A41 and A43, the vector $\dot{\boldsymbol{C}}_{\boldsymbol{C}}\boldsymbol{V}$ can be divided into a centrifugal force component $\boldsymbol{D}_{\dot{\boldsymbol{C}}\boldsymbol{V},\mathrm{CNT}}$ and a Coriolis force component $\boldsymbol{D}_{\dot{\boldsymbol{C}}\boldsymbol{V},\mathrm{COR}}$:

$$\dot{\boldsymbol{C}}_{\boldsymbol{C}}\boldsymbol{V} = \boldsymbol{D}_{\dot{\boldsymbol{C}}\boldsymbol{V},\mathrm{CNT}} + \boldsymbol{D}_{\dot{\boldsymbol{C}}\boldsymbol{V},\mathrm{COR}} \tag{A44}$$

Similarly, the vector $\dot{\boldsymbol{A}}\boldsymbol{V}$ can be decomposed into a centrifugal force component $\boldsymbol{D}_{\dot{\boldsymbol{A}}\boldsymbol{V},\mathrm{CNT}}$ and a Coriolis force component $\boldsymbol{D}_{\dot{\boldsymbol{A}}\boldsymbol{V},\mathrm{COR}}$:

$$\dot{\boldsymbol{A}}\boldsymbol{V} = \boldsymbol{D}_{\dot{\boldsymbol{A}}\boldsymbol{V},\mathrm{CNT}} + \boldsymbol{D}_{\dot{\boldsymbol{A}}\boldsymbol{V},\mathrm{COR}} \tag{A45}$$

The MDT contribution to the generalised acceleration vector is expressed as the sum of individual components including the gyroscopic effect moment component $\boldsymbol{D}_{\dot{\boldsymbol{V}},\mathrm{MDT,GYRO}}$, the segment length fluctuation component $\boldsymbol{D}_{\dot{\boldsymbol{V}},\mathrm{MDT,SG-FLCT}}$, the centrifugal force component $\boldsymbol{D}_{\dot{\boldsymbol{V}},\mathrm{MDT,CNT}}$ and the Coriolis force component $\boldsymbol{D}_{\dot{\boldsymbol{V}},\mathrm{MDT,COR}}$:

$$\boldsymbol{D}_{\dot{\boldsymbol{V}},\mathrm{MDT}} = \boldsymbol{D}_{\dot{\boldsymbol{V}},\mathrm{MDT,GYRO}} + \boldsymbol{D}_{\dot{\boldsymbol{V}},\mathrm{MDT,SG-FLCT}} + \boldsymbol{D}_{\dot{\boldsymbol{V}},\mathrm{MDT,CNT}} + \boldsymbol{D}_{\dot{\boldsymbol{V}},\mathrm{MDT,COR}},$$

$$\begin{cases} \boldsymbol{D}_{\dot{\boldsymbol{V}},\mathrm{MDT,GYRO}} = \boldsymbol{S}_{\dot{\boldsymbol{V}}}\boldsymbol{B}_{\mathrm{sys}}\begin{bmatrix}\bar{\boldsymbol{H}}\boldsymbol{V}\\ \boldsymbol{O}_{9\times1}\\ \boldsymbol{O}_{2\times1}\end{bmatrix}, & \boldsymbol{D}_{\dot{\boldsymbol{V}},\mathrm{MDT,SG-FLCT}} = -\boldsymbol{S}_{\dot{\boldsymbol{V}}}\boldsymbol{B}_{\mathrm{sys}}\begin{bmatrix}\boldsymbol{O}_{18\times1}\\ \dot{\boldsymbol{C}}_{\boldsymbol{B}}\boldsymbol{V}\\ \boldsymbol{O}_{2\times1}\end{bmatrix}, \\ \boldsymbol{D}_{\dot{\boldsymbol{V}},\mathrm{MDT,CNT}} = -\boldsymbol{S}_{\dot{\boldsymbol{V}}}\boldsymbol{B}_{\mathrm{sys}}\begin{bmatrix}\boldsymbol{O}_{18\times1}\\ \boldsymbol{D}_{\dot{\boldsymbol{C}}\boldsymbol{V},\mathrm{CNT}}\\ \boldsymbol{D}_{\dot{\boldsymbol{A}}\boldsymbol{V},\mathrm{CNT}}\end{bmatrix}, & \boldsymbol{D}_{\dot{\boldsymbol{V}},\mathrm{MDT,COR}} = -\boldsymbol{S}_{\dot{\boldsymbol{V}}}\boldsymbol{B}_{\mathrm{sys}}\begin{bmatrix}\boldsymbol{O}_{18\times1}\\ \boldsymbol{D}_{\dot{\boldsymbol{C}}\boldsymbol{V},\mathrm{COR}}\\ \boldsymbol{D}_{\dot{\boldsymbol{A}}\boldsymbol{V},\mathrm{COR}}\end{bmatrix} \end{cases} \tag{A46}$$

Finally, the foot CG's speed can be obtained as the sum of the kinematically-decomposed components as follows:

$$s_{3,\mathrm{MDT}}(k) = D_{s3,\mathrm{MDT,GYRO}}(k) + D_{s3,\mathrm{MDT,SG-FLCT}}(k) + D_{s3,\mathrm{MDT,CNT}}(k) + D_{s3,\mathrm{MDT,COR}}(k),$$

$$\begin{cases} D_{s3,\mathrm{MDT,GYRO}}(k) = \boldsymbol{e}_3^{\mathrm{T}}(k)\bar{\boldsymbol{S}}_3\Delta t\sum_{h=0}^{k-1}\boldsymbol{D}_{\dot{\boldsymbol{V}},\mathrm{MDT,GYRO}}(h), \\ D_{s3,\mathrm{MDT,SG-FLCT}}(k) = \boldsymbol{e}_3^{\mathrm{T}}(k)\bar{\boldsymbol{S}}_3\Delta t\sum_{h=0}^{k-1}\boldsymbol{D}_{\dot{\boldsymbol{V}},\mathrm{MDT,SG-FLCT}}(h), \\ D_{s3,\mathrm{MDT,CNT}}(k) = \boldsymbol{e}_3^{\mathrm{T}}(k)\bar{\boldsymbol{S}}_3\Delta t\sum_{h=0}^{k-1}\boldsymbol{D}_{\dot{\boldsymbol{V}},\mathrm{MDT,CNT}}(h), \\ D_{s3,\mathrm{MDT,COR}}(k) = \boldsymbol{e}_3^{\mathrm{T}}(k)\bar{\boldsymbol{S}}_3\Delta t\sum_{h=0}^{k-1}\boldsymbol{D}_{\dot{\boldsymbol{V}},\mathrm{MDT,COR}}(h) \end{cases} \tag{A47}$$

where $D_{s3,\mathrm{MDT,GYRO}}(k)$, $D_{s3,\mathrm{MDT,SG-FLCT}}(k)$, $D_{s3,\mathrm{MDT,CNT}}(k)$ and $D_{s3,\mathrm{MDT,COR}}(k)$ denote, respectively, the components of the foot CG's speed at time k that arise from the gyroscopic effect moment, segment length fluctuations, centrifugal forces and Coriolis forces.

Figure 1. A block diagram representing the relationships between accelerations arising from the direct and indirect effects of inputs (e.g. joint torques, gravity and other terms) and the generalised acceleration and velocity vectors. Plain arrows indicate multiplication of the input vector with the matrix inside the box to which the arrow is pointing, with the exception of boxes including $\int$,which correspond to a time-integral operation.

Figure 2. A block diagram representing the recurrence formula with respect to the generalised velocity vector. Plain arrows correspond to multiplication of the input vector with the matrix inside the box to which the arrow is pointing. Reshaping Figure 2a into b identifies the contributions due to individual terms $\dot{\boldsymbol{V}}_{\mathrm{Dir}}$, as expressed in Equation 5, at each time instant to the generation of the generalized velocity vector including the motion-dependent processes of the torque inputs arising at any later time.

Figure 3. A block diagram representing the direct and indirect effects of joint torque inputs to the generation of foot segment speed s_3 at time *k*. Plain arrows correspond to multiplication of the input vector with the matrix inside the box to which the arrow is pointing. The highlighted part of individual block diagrams in the direct effect (Figure 3b) and the indirect effect (Figure 3c) show respectively the contributions of the direct and indirect effects of joint torque inputs at time instant *h* to the generation of the foot CG's speed at BC.

Figure 4. Time-curve contributions of the direct and indirect effects of individual terms to the generation of the kicking foot CG's speed $s_3(k)$ for *k*=-200% to 0% (normalised) time. The values shown are the integrated contributions due to the direct and indirect effects of each source from t=-200% to *k*. Each line represents the mean

across the participants at each normalised time, and the white-coloured and shaded regions indicate one standard deviation either side of the mean. Note: the scale in Figures e to h differs from the one in Figures a to d for visual purposes. For clarity, the contributions from gyroscopic effect moments and segment length fluctuations have been omitted from Figure b because the magnitudes of their mean values across the participants were less than 0.14 m/s and 0.4 m/s, respectively, throughout.

Figure 5. Time-curve contribution rates of the direct and indirect effects of joint torque inputs at each instant during the flight and support phases to the generation of kicking-side foot CG's speed at ball contact $s_3(k_{\mathrm{BC}})$. The units of the vertical axis for each graph are m/s per millisecond. These contribution rates indicate the time when, and the specific axis about which, each of the analysed torques induced the foot CG's speed at BC. The white-coloured and shaded regions indicate one standard deviation either side of the mean.

Figure 6. Mean and standard deviation for the integrated contributions from the direct and indirect effects of joint torque inputs during the flight and support phases to the generation of foot CG's speed at ball contact; these correspond to the areas under the respective curves in Figure 5 (pre- and post-SFC, 100%).

Figure A1. A schematic representation of the modelled kicking leg introducing the numbering of the segments (i=0 to 3) and joints (j= 1 to 3), as well as the segmental coordinate systems.